Through thickness residual stress distribution during cold rolling of titanium alloy (commercial-pure)

A dissertation submitted
in partial fulfilment of the requirements
for the degree of

Master of Engineering
in
Production Engineering

by

Ayush Singla
Roll No: 801585006

Under the Supervision of

Dr. Gulshan Kumar
Assistant Professor

MECHANICAL ENGINEERING DEPARTMENT
THAPAR UNIVERSITY, PATIALA

July, 2017

Certificate

I hereby declare that the thesis entitled "**Through thickness residual stress distribution during cold rolling of titanium alloy (commercially-pure)**", is an authentic record of my work carried out as per requirements for the award of the degree of **Master of Engineering** in **Production Engineering** at **Thapar University, Patiala** under the supervision of **Dr. Gulshan Kumar** Assistant Professor, Mechanical Engineering Department, Thapar University, Patiala during July, 2016 to July, 2017. No part of the matter embodied in this report has been submitted to any other university or institute for the award of any degree.

Date: August 17, 2017

Ayush Singla
801585006

It is certified that the above statement made by the student is correct to the best of our knowledge and belief.

17/08/17

Dr. Gulshan Kumar
Assistant Professor
Mechanical Engineering Department
Thapar University, Patiala - 147004

Dedicated

to

my family

For their endless love, support and encouragement

Acknowledgement

I would like to express my deep sense of gratitude and a very sincere thanks to my supervisor **Dr. Gulshan Kumar**, Assistant Professor, at Mechanical Engineering Department, Thapar University, Patiala for his sincere and invaluable guidance which helped me in the accomplishment of this report in the present form. Their dynamic and diligent enthusiasm has been highly instrumental in keeping my spirits high. Their flawless and forthright suggestions blended with an innate intelligent application have crowned my task with success.

I am also thankful to **Prof. Indradev Samajdar**, Department of Metallurgical Engineering and Materials Science, IIT Bombay for allowing me to carried out my measurements at OIM & Texture lab. I also thank **Mr. Khushal Thool,** Research Scholar at IIT Bombay for his help in the measurement of residual stress and microstructure for carrying out my thesis work.

I would like to thank my friends especially my classmates ME (production), Thapar University, Patiala for their immense support during my thesis work.

Ayush Singla

Roll No.: 801585006

List of Figures

List of Tables

Symbols

$d\varepsilon_p$ = Strain rate

σ = Stress in general

μ = coefficient of friction

E = modulus of elasticity, N/mm^2

α = Alpha phase

β = Beta phase

μ = coefficient of friction

Acronyms

HCP = hexagonal closed packed crystal structure

EBSD = electron backscattered diffraction

FE = finite element analysis

FEG = field emission gun

OIM = orientation imaging microscopy

FE = finite element analysis

SEM = Scanning electron microscopy

RD = rolling direction

TD = transverse direction

COF = coefficient of friction

LAB = low angular grain boundaries

HAB = high angular grain boundaries

XRD = x-ray diffraction

Abstract

The main objective of the present dissertation was to observe through-thickness gradient in microstructure and residual stress in titanium alloy (Grade-2) during cold rolling. Cold rolling can be used in order to modify material properties during deformation. The above characteristics were examined using EBSD technique and X-ray diffraction. It was found that rolling leads to microstructure refinement and lowering of residual stress. Maximum compressive residual stress was found to be at top surface (T0) which goes on decreasing as we move towards middle of the specimen. At middle of the specimen (T/2) stresses are near to zero. To confine such through thickness deformation gradients a deformable FE (finite element) model was developed. Conformity was observed between the experimental and the simulation residual stress distributions. Through-thickness residual stress evolution was then extended to see the effect of rolling parameters such as (coefficient of friction and rotational speed). With increasing coefficient of friction and the rotational speed residual stress was increased.

Keywords: Titanium Alloy (Commercially-Pure), Cold Rolling, X-Ray Diffraction (XRD), Electron Back Scatter Diffraction (EBSD), Finite Element Method (FEM).

Table of Contents

Page No.

Chapter 1
Introduction

1.1 General

The residual stress can be defined as the stresses remains in a body, when the body is unacted on by any external agency [1-5]. Figure 1.1a illustrates the creation of residual stress through the deformation of a two phase 'composite' material system – one deforms elastically (phase a) whereas other undergoes an elastic-plastic (phase b) deformation. When the applied stress is released, the (phase a) unloads to zero, (phase b) would be plastically deformed with a strain rate of $d\varepsilon_p$, if the two phases were separate Fig. 1.1b. However, the joining of the two phases led to extension of phase a by phase b and in opposition phase b is compressed by phase a Fig. 1.1c [1].

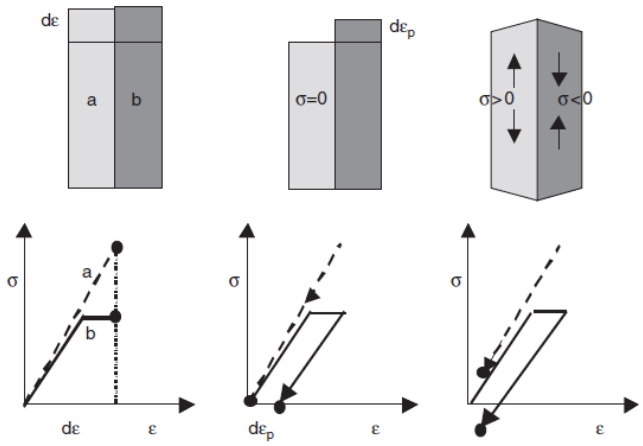

Figure 1.1: Two phase 'composite' material system describing the creation of residual stresses [1].

Residual stress can be classified as:

a. Macroscopic
b. Microscopic

1.1.1 Macroscopic

The stresses varied over several grains of a material component are considered as macro residual stress [1-4]. These are also called as Type 1 (or σ^1) residual stresses [2, 3, 6, 7]. The magnitude of these stresses can be determined by measuring strain in a particular direction at any given point [1, 2]. These can be represented by the uniform distortion of the crystal

lattice, which shifts the diffraction peak. These are continuum level stresses that neglect the underlying microstructure as shown in Fig. 1.2 [4].

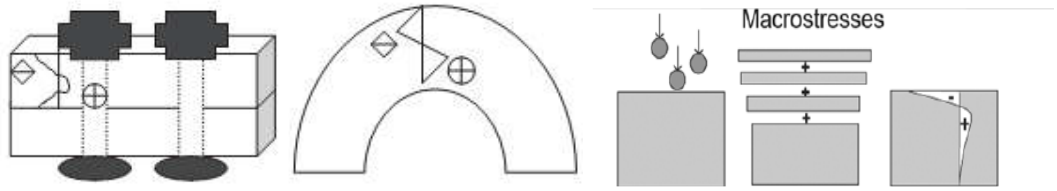

(a) (b) (c)

Figure 1.2: Macroscopic residual stress (a) riveting of two plates [1] (b) bending of bar [1] (c) shot peening [4].

1.1.2 Microscopic

The stresses differ inside the grain due to the presence of inclusion, dislocations, faults, etc. (Fig. 1.3a). These can also differ between the grains or crystallites as shown in Fig. 1.3b [1, 3, 4, 5]. Micro stresses can be classified as Type 2 (σ^2) and Type 3 (σ^3) [2, 3, 6, 7]. Type 2 vary from one grain to another and Type 3 stresses are non-uniform at the sub microscopic level (i.e. atomic distances within a grain) [3].

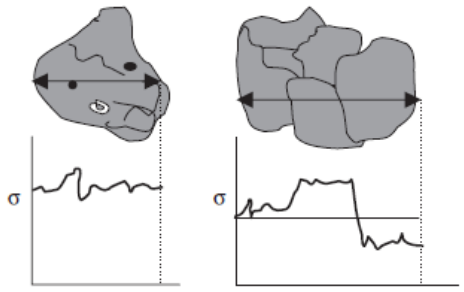

(a) (b)

Figure 1.3: Micro-stresses inside the grains (a) stress can differ inside grains because of the presence of inclusion, dislocations, faults; etc (b) micro stresses differ between different grains [1].

1.1.3 Origin of residual stress

The origin of residual stress can be understood at atomistic level (Fig. 1.4a). The deformation may change interplanar spacing or may incorporate lattice defects [1, 6]. The deformation is induced by the movement of discrete line defects (dislocations) through the crystallite, yield

stress is exceeded on the outer surfaces and the plastic zones expands inwards resulting in residual stress creation as shown in Fig. 1.4 [1, 3, 5, 6].

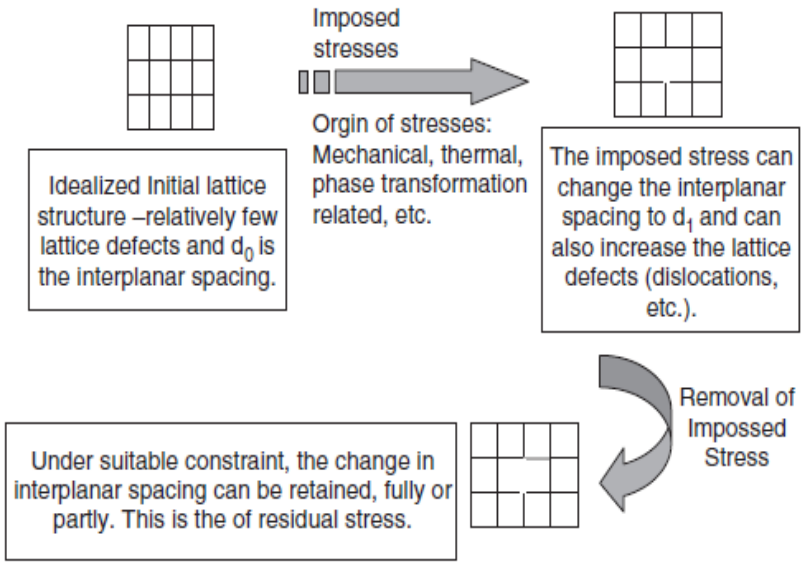

Figure 1.4: An undeformed material with interplanar spacing d_0 is subjected to imposed stresses. The imposed stress can change the interplanar spacing to d_1 and can also increase in lattice defects (dislocations, stacking faults, etc.) [1].

[1].

1.2 Advantages and Applications of Residual Stress

Residual stresses have been a very valuable addition to the field of materials for higher performance [4]. The stresses can be compressive or tensile in nature [1-3]. The compressive residual stresses are being increasingly used in automobile, aerospace, marine, and mineral processing industries owing to their improved specific strength, good wear resistance, higher thermal conductivity, and lower coefficient of thermal expansion. These have been applied to crankshaft or shaft fillets to increase their fatigue strength [4, 5]. The compressive stresses reduce the plastic collapse and fracture as shown in Fig. 1.5a [5, 6, 8]. On the other hand, the tensile residual stress on the surface of component is generally undesirable due to decrease in the fatigue strength, and increase in crack propagation as shown in Fig. 1.5b. These can originates from drawing, machining, welding and grinding which may lead to fatigue failure. The various applications of the residual stresses are shown in Table 1.1.

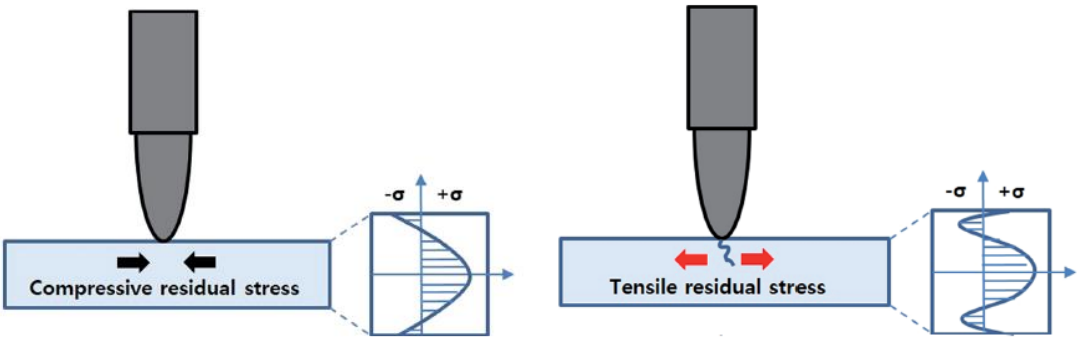

(a) (b)

Figure 1.5: Residual stress (a) compressive residual stress in the skin layer (b) tensile residual stress in the skin layer [8].

Table 1.1: Applications of residual stress.

S.NO.	APPLICATION	TYPE	AUTHOR
1.	Crank Shaft	Compressive	Liou et.al [9]
2.	Shaft Fillets	Compressive	Liou et.al [9]
3.	Turbine Engine	Compressive	Yentzer et.al [10]
4.	Propeller Blades	Compressive	Yentzer et.al [10] Manouchehrifar and Alasvand [11]
5.	Injection Moulding	Compressive	Oh et.al [8]
6.	Connecting Rod	Compressive	https://en.wikipedia.org/wiki/Residual_stress [12]

1.3 Titanium

Titanium was discovered in 1791 by geologist and Pastor Willium Gregor in Cornwall (UK), and later in 1795 named after "Titan" in Greek mythology by German chemist Martin Heinrich Klaproth [13]. Titanium is available in many mineral deposits, mostly in the form of rutile and ilmenite, which are generally distributed in earth's crust and lithosphere. Ti could be extracted by dropping titanium tetrachloride ($TiCl_4$) (see equ.1) and combining $TiCl_4$ with the reducing agent magnesium (Mg) (see equ. 2).

$2FeTiO_3 + 7Cl_2 + 6C\ (900\ °C) \rightarrow 2TiCl_4 + 2FeCl_4 + 6CO$ (1)

$TiCl_4 + 2Mg\ (1100\ °C) \rightarrow 2MgCl_2 + Ti$ (2)

Titanium alloys offers a wide spectrum of strength and combinations of strength and fracture toughness [14]. Figure 1.6 shows the variation of specific strength with ambient temperature in various metal and alloys system. This reflects that the titanium has the highest strength to weight ratio among all mentioned metal and alloy system. It has density of 4.50 g/cm^3 which is lesser than the density of steel and nickel making it suitable for meeting the requirements of low weight and high performance in aerospace/automobile applications (Table 1.2) [3].

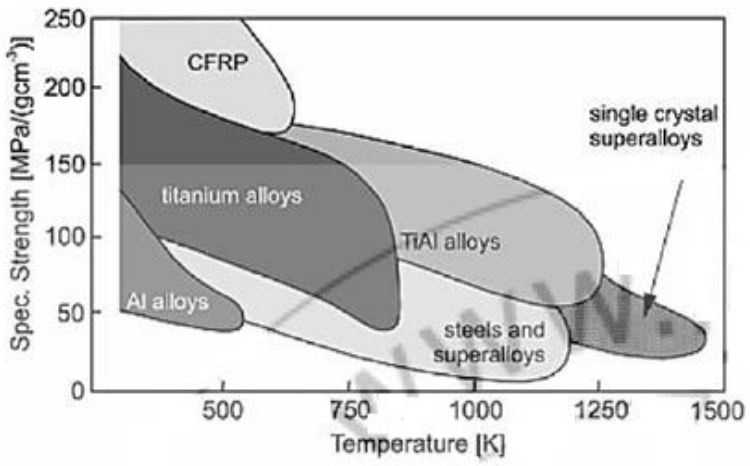

Figure 1.6: Strength to density ratio for different metals and alloys as a function of temperature [15].

Table 1.2: Characteristics of titanium and its alloys in comparison to other structural metallic elements such as Fe, Ni, and Al [3].

	Ti	Fe	Ni	Al
Melting Temperature (°C)	1670	1538	1455	660
Allotropic Transformation (°C)	882 (β → α)	912 (γ → α)	-	-
Crystal Structure	bcc → hcp	fcc → bcc	fcc	fcc
Room Temperature E (GPa)	115	215	200	72
Density (g/cm^3)	4.50	7.90	8.90	2.70
Comparative Corrosion Resistance	Very High	Low	Medium	High
Comparative Reactivity with Oxygen	Very High	Low	Low	High
Comparative Price of Metal	Very High	Low	High	Medium

1.3.1 Titanium alloys:

Titanium alloys are classified into three broad categories: α, α+β, and β alloys depending upon the part of α or β phases present at room temperature. The part of α and β phases can be changed by the accumulation of alloying elements. The alloying elements are categorized as α stabilizers and β stabilizers depending on whether they increase, decrease, or contain no effect on the β transus temperature respectively [16]. This effect is shown schematically in Table 1.3.

Table 1.3: Typical amounts and effect of alloying elements commonly added to titanium [17].

Alloying element	Effect on structure
Al	α stabilizer
Sn	α stabilizer
C	α stabilizer
N	α stabilizer
O	α stabilizer
V	β stabilizer
Cr	β stabilizer
Mo	β stabilizer
H	β stabilizer
Zr	α- β stabilizer

1.4 Cold Rolling

The era of rolling started during fourteenth century: with the undersized band, over driven rolls used for flattening gold and silver plates. However, the first proper rolling mill was projected by Leonardo da Vinci in 1480 [18]. The rolling of the sheet metal (for both ferrous and nonferrous materials) was not proficient during this period. Later in 1682, a large rolling mill was developed for hot rolling of ferrous materials at Swalwell and Winlaton in England [18]. In 1697, a rolling mill for producing thin iron sheets was designed by John Hanbury [19]. In 1776, Richard ford patented a tandem mill, in which metal workpiece was rolled in successive stands, for making plates and sheets [18]. The modern practices can be attributed to the revolutionary efforts for his use of grooved rolls for rolling iron bars came to existence

with the efforts of Henry Cort in 1783 [18]. The advancement of technology led to the development of modern rolling mills.

It is a most widely used metal forming process of metals to obtain slabs, plates, sheets, bars and other structural parts [18]. In this process, a work piece is passed from a pair of roller to reduce the thickness and to maintain the uniformity of the work piece. The gap between the rollers must be less than the material thickness [20, 21]. The frictional force provided on the contact surfaces pushed the sample into the roll assembly as shown in Fig. 1.7.

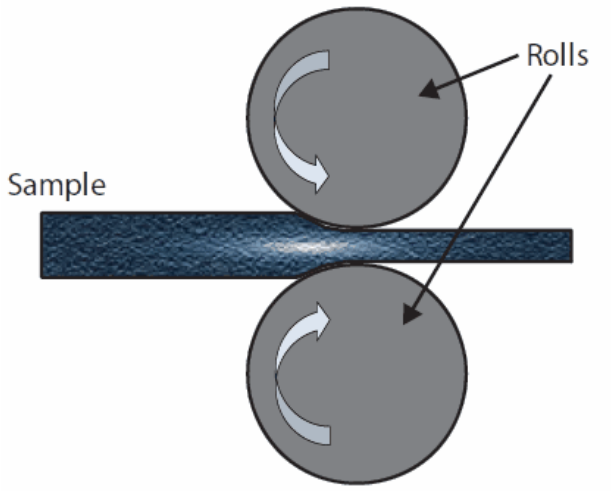

Figure 1.7 Cold rolling process [22].

1.5 Applications

Cold rolling produces good surface finish, improves the physical properties of the metal such as tensile strength, and reduces the material thickness to precise gauges. It enhanced the fatigue life, increases the strength characteristics, and improves the surface finish of a material component [20]. Cold rolled products are being increasingly used in automobile, aerospace, marine, and mineral processing industries owing to their improved specific strength, good wear resistance, higher thermal conductivity, and lower coefficient of thermal expansion [20, 21, 23, 24]. The various applications of cold rolling are bridges structures, ships, large diameter pipes, storage tanks, boilers, railway wagons, pressure vessels, and weather proof plates for the construction of railcars [24].

1.6 Motivation

One of the main challenges for automobile and aerospace industries is to reduce the impact of burning fossil fuels in the environment. A lot of research has been done on minimizing the fuel consumption in automobiles and aircrafts, which can be achieved, by reducing the weight

of the vehicles. Due to this, materials with higher strength are preferred. Titanium has high strength to density ratio, high corrosion resistance, and the ability to withstand high temperatures. It is used in engine applications such as rotors, compressor blades etc. The residual stresses are induced into rotors, compressor blades from various manufacturing and thermal processes, such as forming, machining, thermal loads etc. These processes will result into the creation of tensile residual stresses. The tensile residual stress in the component is generally undesirable as they decrease the fatigue strength, and increases the crack propagation. Due to the occurrence of residual stresses, single point failure in a propeller blade can cause great loss to the aircraft. To give a useful fatigue life, the critical blade is cold rolled to bring in compressive residual stresses in the depth [10]. The residual stress has been calculated over the surface till now, it is not being calculated through the thickness. However, the stress has been gone through the thickness due to which gradient has been occurred. That is why the proposed research work was planned to investigate the effect of "through thickness residual stress distribution during cold rolling of titanium alloy (commercial-pure)".

1.7 Summary

This chapter started with a brief introduction of residual stress. Further, different types of stresses, its origin and commercial applications have been explained. An emphasize on titanium and its alloys have been given being the material used for the present research work. The cold rolling process used to deform the titanium alloy in the present work has been also introduced briefly in this chapter. In the last section motivation has been briefly introduced.

1.8 Organization of report

This report is divided into six main chapters. In Chapter 1, general introduction of the work is explained briefly. Chapter 2 contains the comprehensive literature review related to the problem along with general theory of microstructure and mechanical properties of titanium. Chapter 3 describes the characterization techniques used for carrying out the experimental work. Chapter 4 contains the details about the finite element modelling of the cold rolling. The chapter 5 includes the results and discussion of the residual stress gradient during cold rolling of titanium alloy. The experimental results were further validated with the FE Simulated results. The chapter 6 summarized the present work and provided the future scope for further research.

Chapter 2

Literature Review

2.1 General

This chapter presents a detailed review of literature with regards to microstructure (twinning, various types of twinning, and slip deformation process), Texture and resulting mechanical properties (Young's modulus, Strength, and Elongation) of titanium alloy.

2.2 Literature Review

Yoo [25] investigated the role of twinning in hexagonal close packed (HCP) metals. Deformation twinning, is one of the mode of deformation in crystals, becomes prevalent only at high strain rates or low temperatures. Twinning plays an important role in maintaining a generalized plastic flow of polycrystals at all temperatures. It has been observed that the deformation twinning can efficiently strengthen a material. Hexagonal metals show a significant variation in strength and ductility. Based on the cohesive energy, the simple metals (Mg, Zn) are quite weak; the transition metals (e.g., Ti, Zr) are strong. Ductile metals such as Ti, Zr etc. showed a twin expansion in both tension and compression state. On the other hand, metals with limited ductility twinned only through tension. It has been showed that twinning plays an important role in strengthening of material by maintaining its plastic flow. The process of slip dislocations into twins and the resulting twin growth varying occur among hexagonal metals e.g. easy for Cd, and Zn relative to the Ti and Zn.

Nourbakhsh and O'brien [26] studied the microstructure and texture formation during cold rolling in (CP-Ti). Sample was cold rolled to different strains in the range 20% to 80%. Titanium deforms primarily by twinning at low strains (twinning decreases with increasing strain), whereas at strains above 40% it deforms by slip [27]. At high deformation, microstructure consists of highly elongated grains, with high density of dislocations of grains [1]. The evolution of texture in titanium is rapid. At 20% strain a split rolling direction texture forms, and strain at 40% texture change from split rolling direction to split transverse direction as shown in Fig. 2.1(a–b) [28].

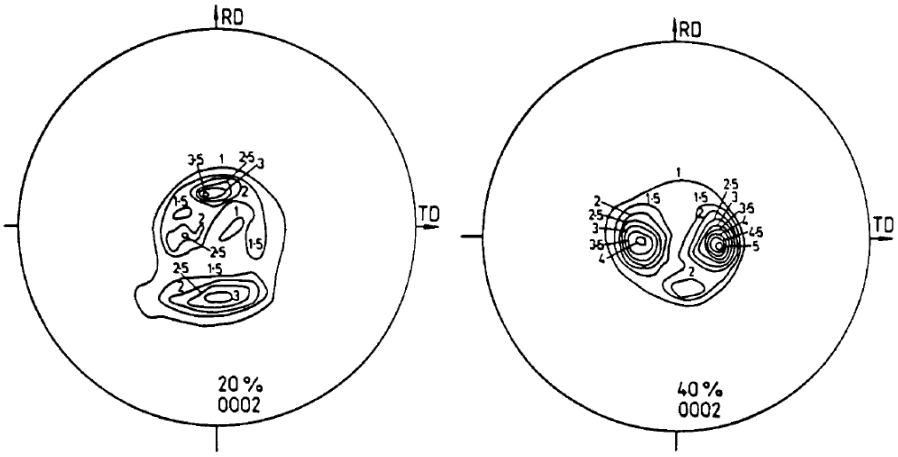

(a) (b)

Figure 2.1: {0002} pole figures (a) cold rolling to a strain of 20% (b) cold rolling to a strain of 40% [26].

Philippe et al. [29] investigated the mechanical twinning and its role in the texture development during cold rolling of titanium and zirconium sheets. Material twinning achieves the reorientation of the grains. Lots of twins were observed in the material deformed by rolling up to 50% of deformation (twins can hardly be recognized after 50% deformation). It is showed that twins of the compressive and tensile nature appear in the samples stretched parallel to the rolling direction. The textures of the titanium specimens are similar but for those which have high O_2-content. The {0002} pole figures show two strong maxima at 35° inclined towards transverse direction and {1010} shows a preferred orientation parallel to rolling direction (Fig. 2.2). The {0002} of the samples with higher O_2-content (T25$O_2$4Fe-2500 ppm 02) show a smaller tilt angle towards transverse direction, and weak maxima inclined towards rolling direction (Fig. 2.3).

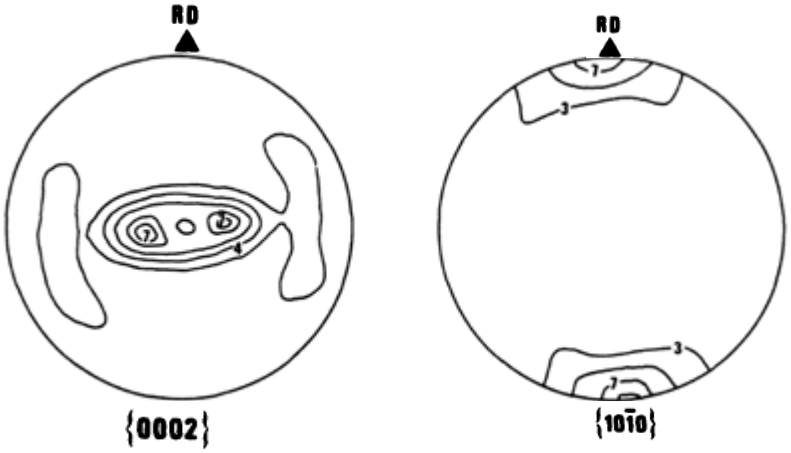

Figure 2.2: Pole figures {0002} and {1010} after 50% cold rolling for T35 [29].

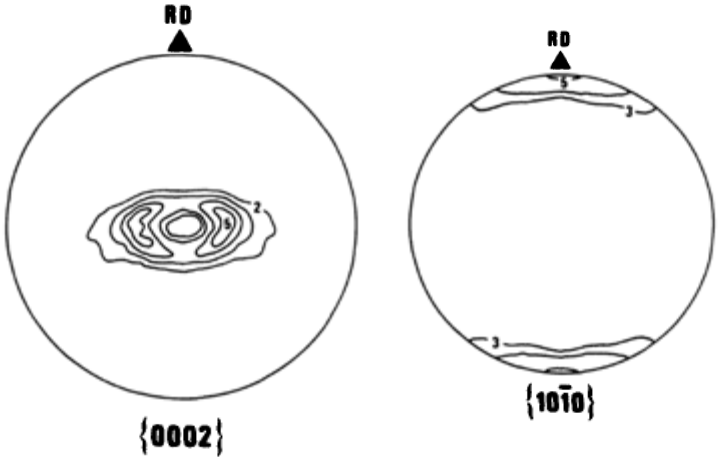

Figure 2.3: Pole figures {0002} and {1010} after 50% cold rolling for T 250$_2$4Fe [29].

Nishitani et al. [30] investigated the twinned crystals of polysynthetically TiAl rolled at room temperature. The maximum reduction in thickness which is likely without fracture depends on lamellae orientation with respect to the rolling direction. The maximum reduction in thickness which was possible without fracture for specimens of both the parallel (Fig. 2.4a) and perpendicular types (Fig. 2.4b) of lamellae lie at an angle ɵ from the rolling direction are shown in Fig. 2.5. It has been showed that length strain is most frequent for the perpendicular type specimen, whereas width strain is least frequent for the parallel type specimen as shown in Fig. 2.6.

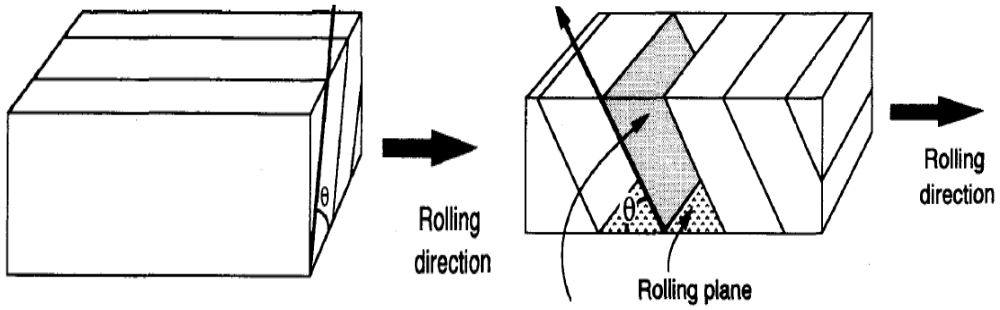

Figure 2.4: Lamellae orientation with respect to the rolling plane (a) parallel and (b) perpendicular types [30].

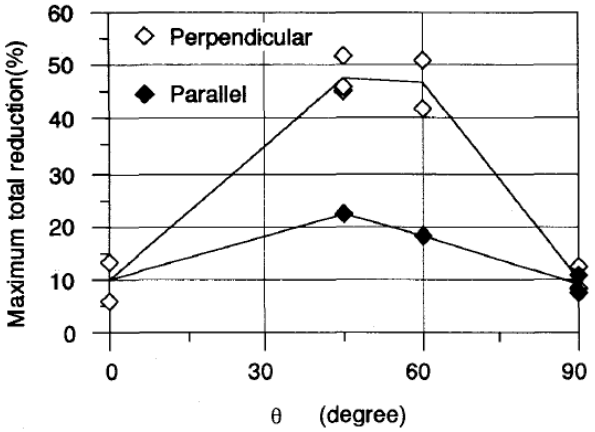

Figure 2.5: The maximum reduction in thickness for specimens of the parallel and perpendicular types with four different angles [30].

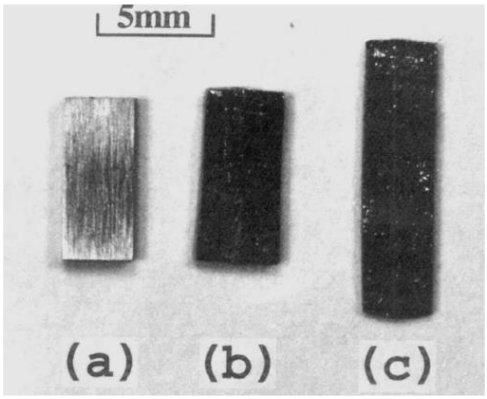

Figure 2.6: Shapes of a specimen (a) before rolling (b) parallel type 20% rolled, and (c) specimen of the perpendicular type 45% rolled [30].

Chun et al. [31] investigated the microstructure evolution and texture development during cold rolling of commercial pure titanium (CP-Ti). The deformation of the material was carried out by the activation of slip or twinning. Twinning plays an important role in deformation and texture formation [26, 29]. The initial structure has equiaxed grains with an average grain size of 30 μm. As the deformation increased from 10% to 20% in thickness direction, the fraction of twins gradually starts increasing as shown in Fig. 2.7(a) and (b) respectively. At higher reductions of 30% and 40%, an essential refinement of the microstructure was observed in the grains (Fig. 2.7(c-d)). The grains marked with NT reflect the deformation by slip and the grains without NT showed twinning (Fig. 2.7(c–d)). The deformation was accommodated by slip and twinning till 40% reduction in thickness. However, the slip was predominant at higher deformation (Fig. 2.8). The secondary as well as tertiary twins induced in the existing twins were activated in the favorable orientation with

increase in deformation. Deformation also leads to the formation of low angular boundaries (LABs). The boundaries with misorientation less 15° are considered as low angle grain boundaries or sub-grain boundaries. The fraction of low angle boundaries was 27% after 10% reduction (Fig. 2.9a), 51% after 20% reduction (Fig. 2.9b) and 68% after 30% reduction (Fig. 2.9c). The LABs increase till 40% reduction as shown in Fig. 2.9d. This study showed that the activation of deformation twinning results in grain refinement due to the formation of secondary and tertiary twins.

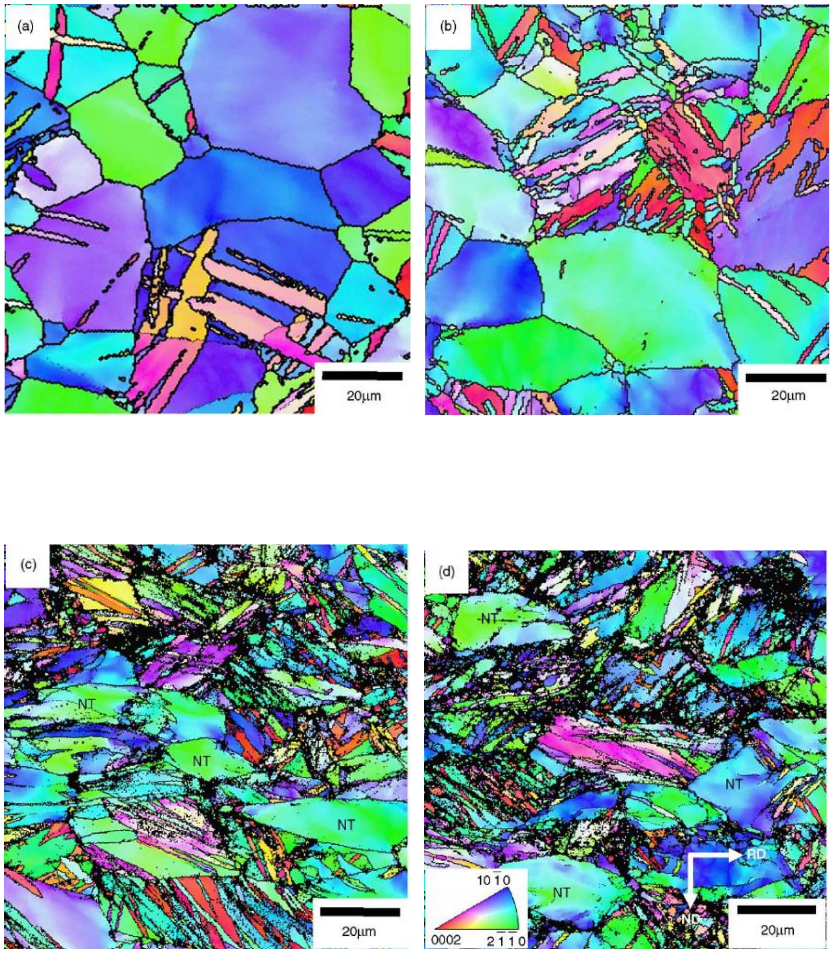

Figure 2.7: EBSD for the RD direction of CP-Ti cold rolled to thickness reductions of (a) 10%, (b) 20%, (c) 30% and (d) 40%. In (c) and (d), NT indicates grains without twins [31].

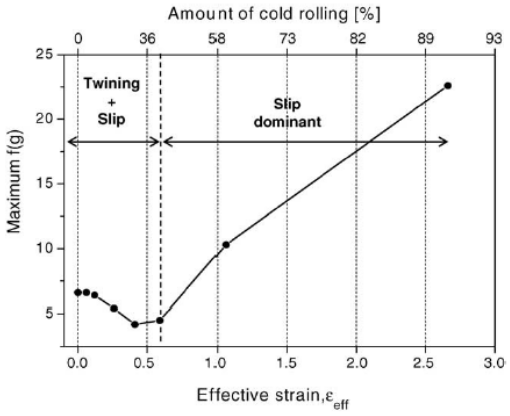

Figure 2.8: For low to intermediate deformation, thickness reduction less than 40% was accommodated by slip and twinning [31].

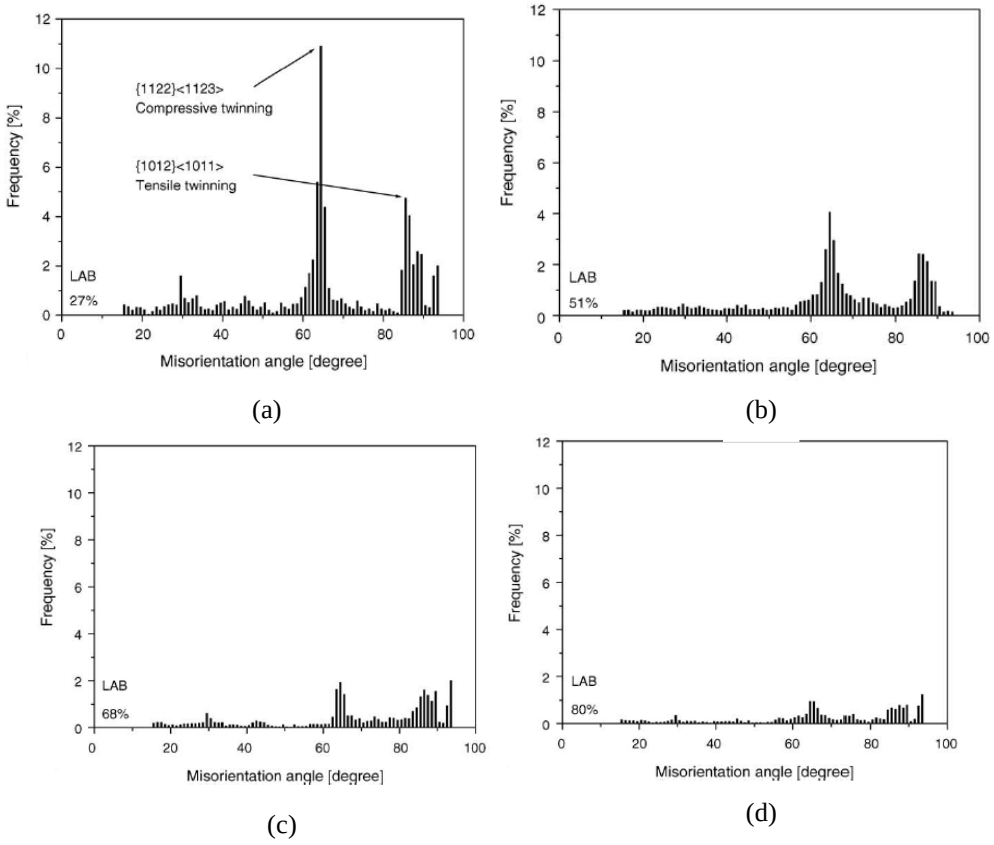

Figure 2.9: Fraction of LAB at (a) 10%, (b) 20%, (c) 30% and (d) 40% deformation [31].

Zhou et al. [32] examined the microstructure of beta titanium alloy. Beta titanium alloy has better plastic formability than the alpha alloy or α+β alloy. Microstructures of both as received and cold-rolled specimens are shown in Fig. 2.10. The gap between the bands of the initial structure (Fig. 2.4a) is greater than the cold rolled structure (Fig. 2.4b) [32]. This study

showed that the band like trans granular structure is caused by the segregation of the beta stabilizing elements.

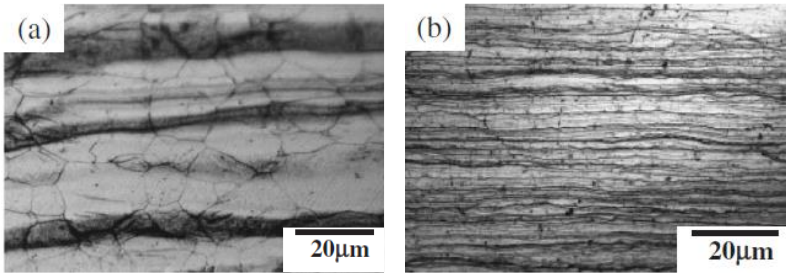

Figure 2.10: Optical micrographs of the (a) as-received and (b) cold-rolled [32].

Bozzolo et al. [33] investigated the texture and microstructure development during cold-rolling of commercial pure titanium (CP-Ti). The starting material is in the fully recrystallized state. The microstructure evolution with cold rolling is shown in Fig. 2.11(a–c). The initial microstructure showed the equiaxed grains with an average grain size of 30 μm (Fig. 2.11a). The fraction of twins increasing after 25% deformation (Fig. 2.11b) and twinned areas are subdivided into small features after 50% deformation as shown in Fig. 2.11c. The microstructure obtained after 80% reduction through cold rolling can be divided into two different parts: (1) 85% volume of the titanium is highly misoriented and the others (2) 15% volume consist of lamellar structure, which deformed only by slip did not show twinning (Fig. 2.12). The deformation weakens the texture, the (0001) maxima spread out and the {10–10} maximum shifts towards the rolling direction from starting material to 80% cold rolled material as shown in Fig. 2.13. This study showed that the twinning plays an important role in the grain disintegration. Multiple twinning is an efficient mechanism of grain fragmentation in the beginning of deformation. The twins are further fragmented into increasingly smaller domains by slip system.

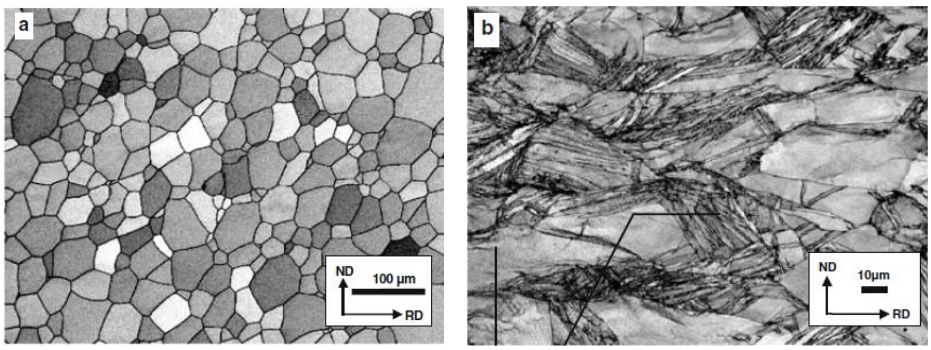

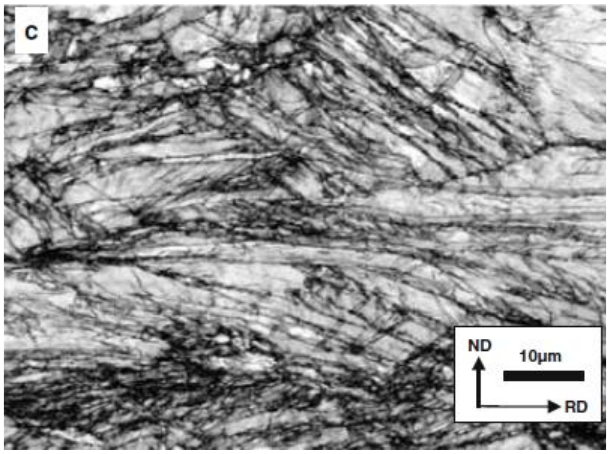

Figure 2.11: Microstructure generation upon cold-rolling (a) received material: equiaxed grained. (b) 25% cold rolling areas (c) after 50% cold rolling [33].

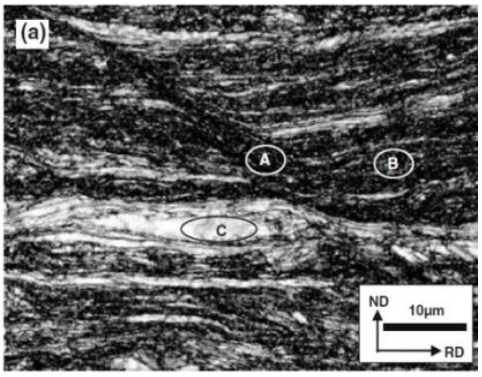

Figure 2.12: Cold rolling can be divided into two different parts: (A and B) 85% volume is fine-subdivided with greatly misoriented and the others (C) 15% volume consist in structures of lamellar [33].

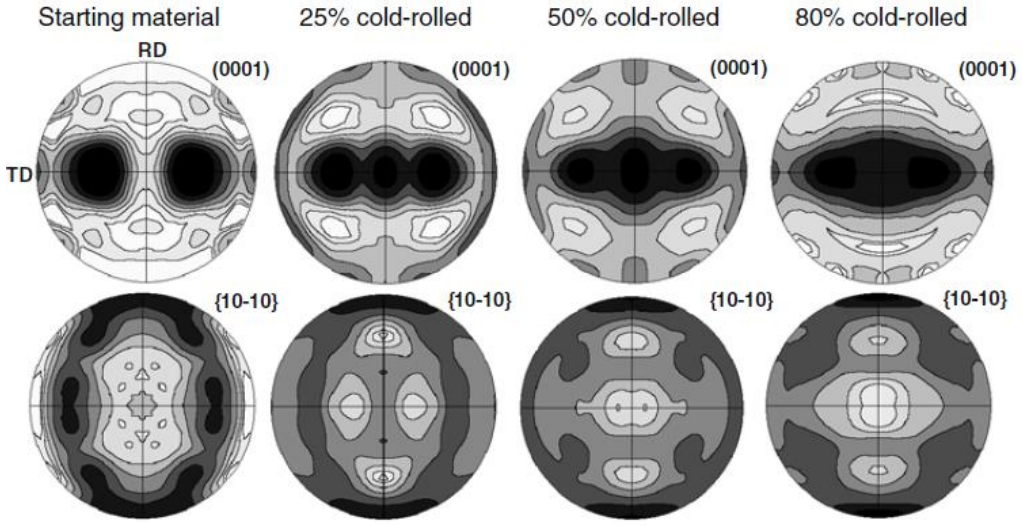

Figure 2.13: Texture generation upon cold-rolling (a) starting material: equiaxed grained. (b) 25% cold rolling (c) after 50% cold rolling (d) after 80% cold rolling [33].

Gonzalez et al. [34] studied the effect of cold work on the martensitic transformation and on the apparent modulus of elasticity in titanium alloy (Ti-21.6Hf-23.7Nb-1Zr). Titanium was deformed from 5% to 95% and characterized by the microstructure and mechanically. Elastic modulus was evaluated by nanoindentation instrument with a berkovich and a spherical tip respectively as shown in Fig. 2.14. Down grading in the elastic modulus was observed when cold work percentage increased (Fig. 2.14). This study showed that a high amount of martensite was found in the low cold work percentages as compare to the unprocessed material because martensitic transformation was formed at 5% and started to fade away after the 10% of cold work. Cold working results in disappearance of the martensite until the recrystallization phase took place after the 75% of cold work as shown in Fig. 2.15.

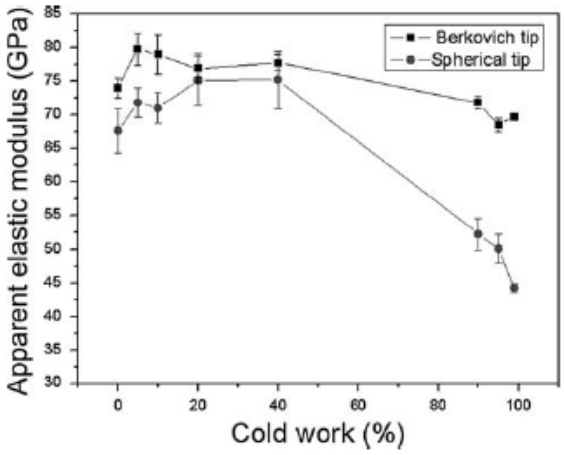

Figure 2.14: Apparent elastic modulus vs. cold work percentages calculating by using a Berkovich and a spherical tip [34].

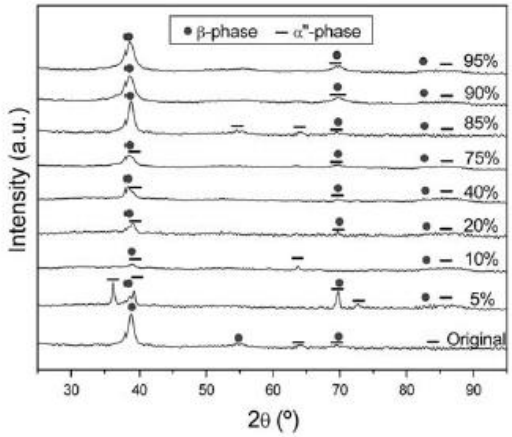

Figure 2.15: X-ray diffraction patterns of the quenched alloy and after different cold-roll percentages [34].

Lei bao et al. [35] have observed the significance of twinning during cold rolling of commercial pure titanium (CP-Ti). The material was deformed up to 30% in thickness direction to determine the individual rotation of grains. The role of mechanical twins during the thickness reduction of 10% and 20% has been emphasized in this study. Different types of twin systems were activated: tensile twinning {1012}, compression twinning {1122} [14]. Evolution of secondary twins {1012} occurs when the crystallographic-axis orientates the tensile twinning of the tensile twins. Only small amount of second order twins have been observed. No twins were found in as received material (Fig. 2.16a). A misorientation of 65° occurs at 10% deformation, suggesting the compressive twinning is prime at this deformation stage (Fig. 2.16b). Tensile twinning, on the other hand, remarkable increased with increase in deformation to 20% (Fig. 2.16c). It is also showed that the formation of the secondary twin inside the primary twin results from the reorientation of the c-axis.

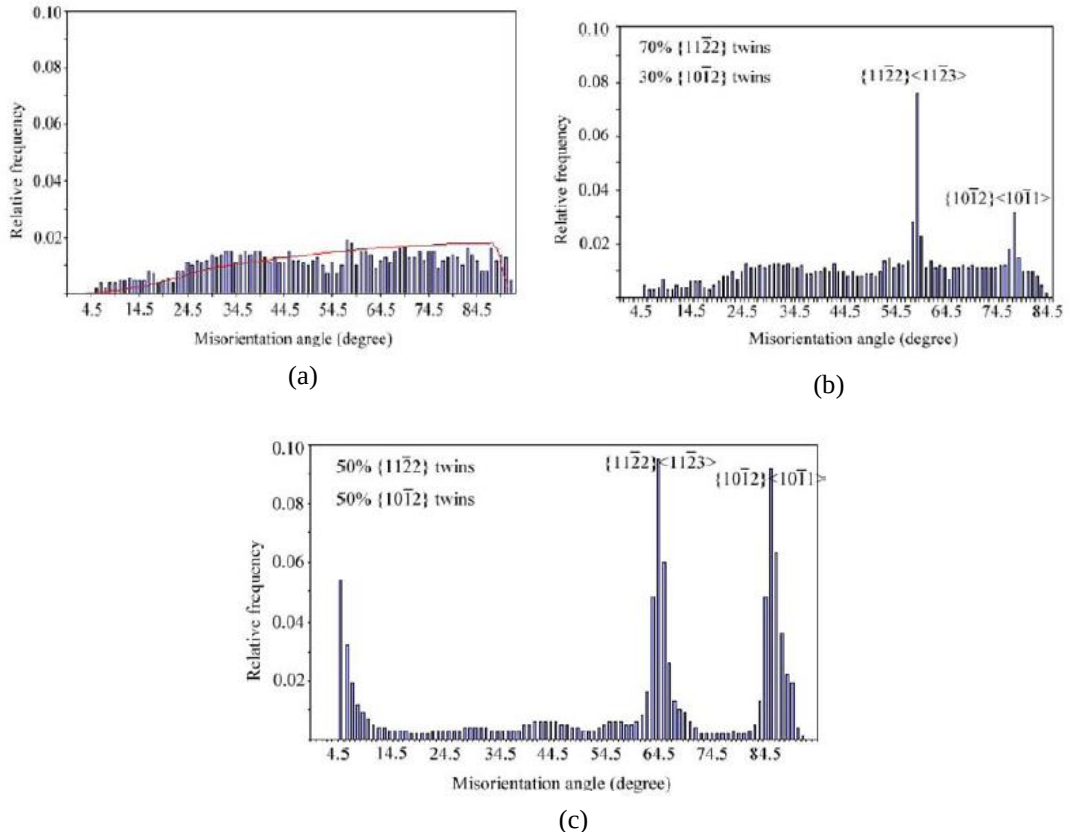

Figure 2.16: Effect of cold rolling at (a) as received, (b) 10% deformation, (c) 20% deformation [35].

Zherebtsova et al. [36] quantified the microstructure evolution during cold rolling of commercial pure titanium to a thickness reduction of 93%. In this study, the grain size and the boundary density was analyzed. The density of high-angle boundaries as a function of thickness strain has three different stages, each of which has a different mechanism of microstructure formation such as: (i) twinning of grains, (ii) enhance in dislocation density and (iii) development of deformation induced high-angle boundaries. The initial microstructure showed the equiaxed grains with an average grain size of 15 μm (Fig. 2.17a). After 40% deformation, a large number of twins were observed (Fig. 2.17b). Cold rolling to 93% deformation led to refinement of the microstructure and increase in dislocation density (Fig. 2.17c). An increase in the fraction of LABs observed with an increase in thickness reduction to 40%. However, with further cold rolling to thickness reduction 93%, the fraction of HABs increased as shown in Fig. 2.18.

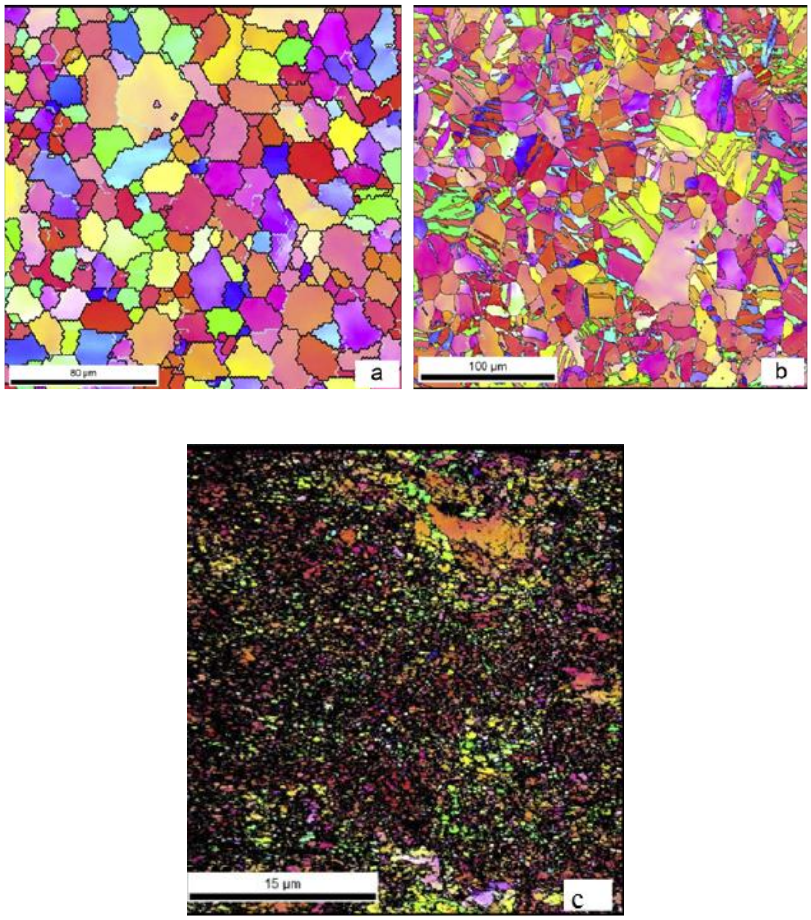

Figure 2.17: Cold rolled titanium samples (a) as received, (b) 40% deformation, (c) 93% deformation [36].

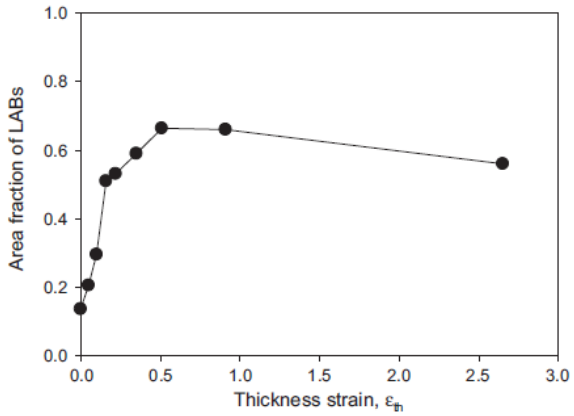

Figure 2.18: Formation of low angle boundaries and parallel increase in low angle boundaries misorientations to high angles boundaries [36].

Zhao et al. [37] studied the effect of deformation on mechanical properties of β-type titanium alloy (ω phase transformation and mechanical twinning). In this study, the microstructures, Young's modulus, and tensile properties of the material were examined. Mechanical twinning can occur in any alloy during cold rolling. The Young's modulus of the alloy increases because of the deformation of induced ω phase with cold rolling. The amount of ω phase decreases with increasing the β stabilizer. β stabilizer increases with increasing cold reduction. It is showed that the major increase in tensile strength is recognized by the combined effect of the deformation induced change of ω phase and work hardening during cold rolling.

Tripathi et al. [38] have shown the fatigue behaviour of commercial pure titanium during cold rolling. In this study, the samples were cold rolled to a thickness reduction of 2.5, 5, 7.5 and 10%. The cold rolling significantly improved fatigue life of the material. It is observed that there is dual slope in the as received condition where as there is only single slope in the cold rolled material. Fatigue life of the material is considerably improved at low deformation. This effect of cold rolling in improving fatigue life, at low deformation is attributed to higher resistance against the crack initiation. It has been showed that even low degree of cold working (5%) is effectual in improving fatigue life of the titanium alloy as shown in Fig. 2.19.

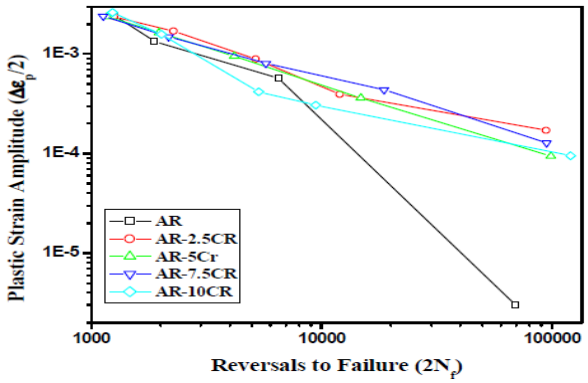

Figure 2.19: Plots for titanium metal in different strain [38].

Wronski et al. studied the microstructure and residual stress in asymmetrically rolled (Ti-grade 2). Asymmetry rolling was done with two identical rollers, driven with different angular velocities ω_1 and ω_2. Asymmetric rolling leads to microstructure refinement and lowering of residual stress. The initial material (Fig. 2.20a), symmetrically rolled ($A=\omega_1/\omega_2=1$) (Fig. 2.20b) and asymmetrically (A=1.5) (Fig 2.20c) rolled samples. It is seen in Fig. 2.20c that microstructure is finer in the asymmetrically rolled material. This is confirmed in Fig. 2.21, where the average grain size is minimum for (A=1.5). We see that with increasing rolling asymmetry, the grain area is decreasing. Residual stresses were calculated on 'top' and 'bottom' surfaces of samples. Two titanium samples were examined: rolled symmetrically, A=1, and asymmetrically, A=1.5 (80 % rolling reduction). It is showed that the values of residual stress components are significantly lower in asymmetrically rolled samples as shown in Table 1.4.

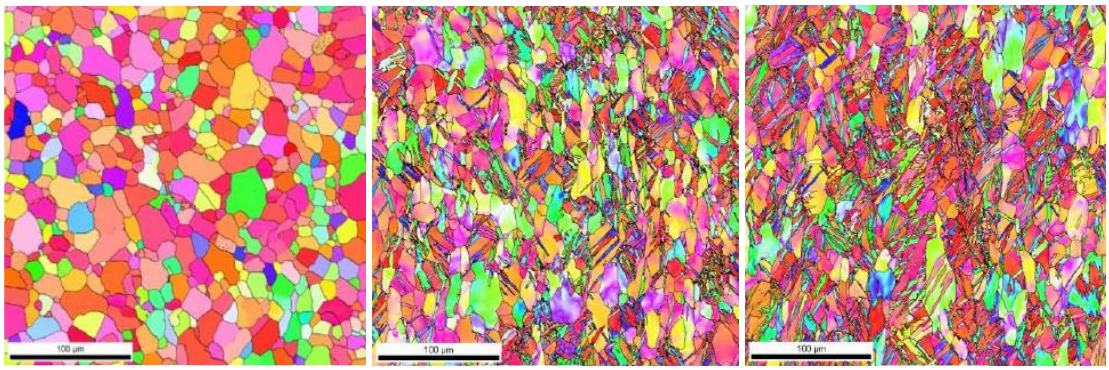

(a) (b) (c)

Figure 2.20: Microstructure of (a) initial material , (b) symmetrically (A=1) and (c) asymmetrically (A=1.5) to the reduction of 20 % [39].

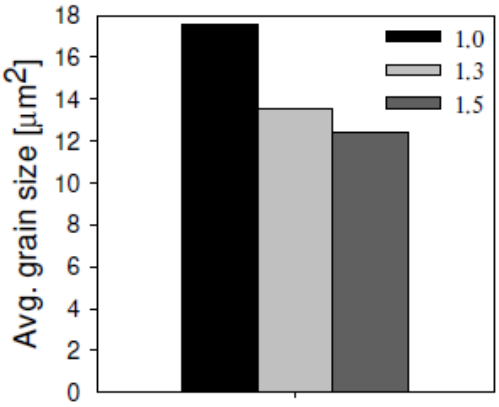

Figure 2.21: Influence of asymmetric rolling (A=1, A=1.3 and A=1.5) [39].

Table 2.1: Effect of residual stress (A=1, A=1.5) [39].

	Top surface		Bottom surface	
	σ_{11}	σ_{22}	σ_{11}	σ_{22}
$A=\omega_1/\omega_2=1$	- 87.8 ± 18	-128.6 ± 18	-108.6 ± 18	-165.9 ± 18
$A=\omega_1/\omega_2=1.5$	- 60.4 ± 14	- 104.2 ± 14	- 37.7 ± 18	- 37.4 ± 18

Jaroslav et al. [40] investigated the effect of cold rolling on microstructure and mechanical properties of beta titanium alloy. Beta titanium alloys are widely used for hard tissue replacements due to their properties, high strength and low modulus of elasticity. The work pieces were imposed with a strain of 40%, 60%, 80% and 93% in thickness direction. The microstructure after cold rolling to 60% has elongated grains in the direction of rolling. Deformation twins and bands can be observed inside these grains as shown in Fig. 2.22. It has been observed that the tensile strength improved from 600 to 850 MPa (Fig. 2.23a) with thickness reduction. On the other hand, the elongation drops down to 9% (Fig. 2.23b). The modulus of elasticity has been increased within range of 45 to 55 GPa (Fig. 2.23c). The strength to modulus ratio increases with thickness reduction and young's modulus starts decreasing as thickness reduction increases.

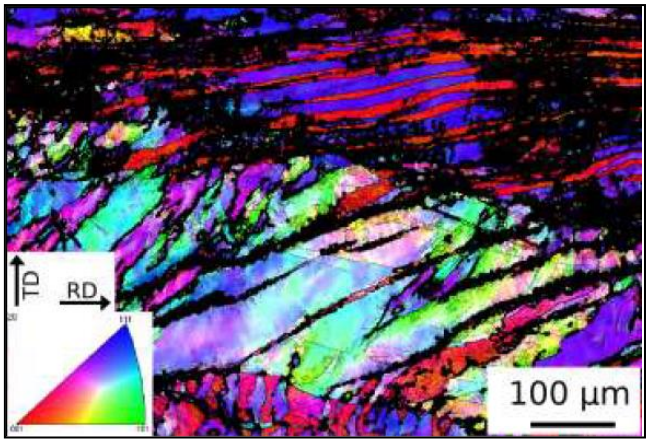

Figure 2.22: Twins and deformation bands in 60% deformation [40].

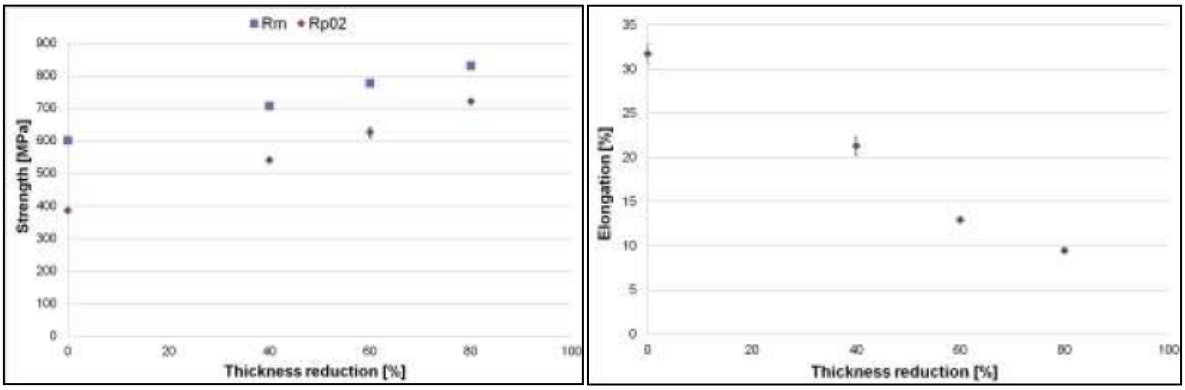

(a) (b)

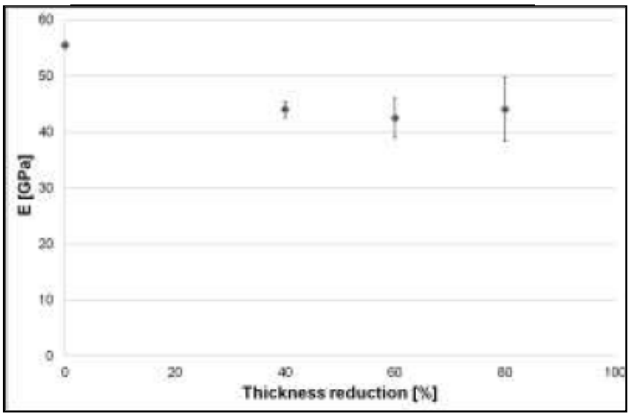

(c)

Figure 2.23: Comparison of (a) tensile strength, (b) elongation and (c) young modulus [40].

2.3 Summary of the literature review

It was observed that cold rolling improved the mechanical properties and wear. It has been showed that even low degree of cold working is effectual in improving fatigue life of the titanium alloy. The strength to modulus ratio increases with thickness reduction and young's modulus starts decreasing as thickness reduction increases. Reason behind is higher cold-rolling reduction leads to a higher density of dislocations, dislocations led to residual stress if residual stress occurs hardness increases. Refinement of microstructure improved the amount of equiaxed grains and the evolution of thin substructure. It was also observed that due to misorientation distributions the fraction of low angle boundaries increased with increasing deformation and secondary twins was observed above 20% thickness reduction.

2.4 Gaps in the existing literature

A vast literature is available on the effect of cold rolling on microstructure and mechanical properties of commercial pure titanium. No work has been reported to study the effect residual stress in titanium alloy during cold rolling. The proposed research work was planned to investigate the effect of *"Through thickness residual stress distribution during cold rolling of titanium alloy (commercial-pure)"*. However, the following limitations have been observed after a detailed literature review.

- Through thickness residual stress gradient during rolling in titanium alloy.
- Residual stress distribution on the surface along longitudinal and transverse direction.
- Residual stress variation with respect to coefficient of friction and roller speed.

Chapter 3

Design of the Study

3.1 General

This chapter discusses the overall design of the study which includes constituent materials of the alloy, and methodology. The chapter also covers the details of machines and equipment used for the experimental work.

3.2 Starting material

As-received titanium alloy (grade-2) was used for the measurement of the residual stress through thickness. Table 3.1 presents the chemical composition of titanium grade-2 alloy. It was purchased from Manhar Metal Private Limited, Mumbai, India.

Table 3.1 Chemical composition of Titanium Grade-2 alloy.

Elements	Fe	C	Cr	Mn	Al	V	Ti
Wt. %	0.14	0.04	0.02	0.09	0.09	-	99.62

3.3 Methodology

Commercial titanium alloy (grade-2), with chemical composition listed in Table 3.1, was used. The base material, (300×100mm) with 8.4 mm thick strip was cold rolled to 20%, 40% and 60% reductions in a laboratory rolling mill. The rollers were 180 mm in diameter and rotating at a uniform rotational speed of 10 rpm. Rolled samples were carefully polished (finishing with sub-micron SiC paper and then electro-polishing) to different thickness locations. These were T/11, T/7, T/5, T/4, T/3 and T/2 (centre of the rolled sheet), where T represents the total thickness of the rolled sheet. Controlled electro-polishing was used: an electrolyte of 80:20 methyl alcohol and perchloric acid at 27V, 4.5A current for 10 sec. Detailed characterizations, by X-ray and electron diffraction, were carried out on the rolling plane at the surface and at these thickness locations. The residual stresses were measured through X-ray diffraction. The X-ray measurements were made in a Bruker^{TM} system. In this study, measurements were made for both $\sigma 11$ and $\tau 13$. The through thickness microstructure

evolution was also characterized through electron backscattered diffraction (EBSD). The EBSD scans were performed in a Quanta 3D FEG (Field emission gun) using a OIM EBSD package software. For each specimen and thickness location, an area of 100 X 150 µm was covered at a step size of 0.1 µm. Figure 3.1 presents the flow chart of the methodology used for the processing, characterization, and testing of cold rolled Grade-2 Ti alloy.

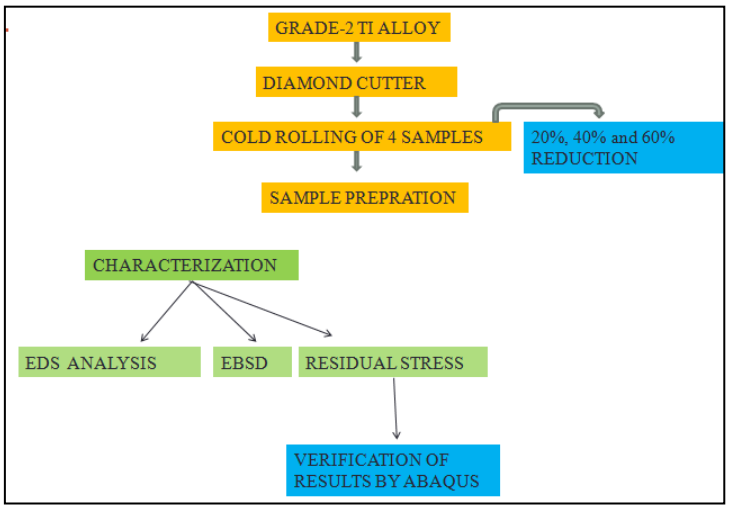

Figure 3.1: Flow chart of the methodology to be used for the proposed research.

3.4 Machines and equipment

3.4.1 Diamond cutter

Diamond cutter (Make: Struers, Danish) was used for cutting the material. Specimen was cut into 4 equal pieces for different rolling reductions.

Figure 3.2: Diamond cutter (Courtesy: IIT, Bombay).

Cutting was carried out at 0.5mm/rev. Figure 3.2 presents the schematic of diamond cutter.

3.4.2 Rolling mill

Rolling mill set-up was used to roll the titanium grade-2 from 0% to 60%. The rollers of approx. 180 mm diameter were used to roll the material. The rolling mill was carried out at 10 rpm to achieve the desired sample reductions. Figure 3.3 presents the schematic of rolling mill apparatus.

Figure 3.3: Rolling mill (Courtesy: IIT, Bombay).

3.4.3 Grinding

The surface to be examined by EBSD was polished with abrasive papers of successive finer grades such as 400, 600, 800, 1000, 1200, 1500 and 2000 mesh abrasive paper (Fig. 3.4). Each time the sample was rubbed on SiC paper, scratch marks were introduced, therefore polishing was continued till all the scratches were in one direction. Then, the next paper with finer grade was used with direction of rubbing switched perpendicular to previous scratches. Similar process was repeated from the coarse grade paper (400 grit size) up to fine grade paper (2000 grit size). Over-heating of sample was avoided so that no modification in the microstructure occurs. Pressure needs to be adjusted, as high pressures can introduce deep scratches whereas low pressures result in long time consumption.

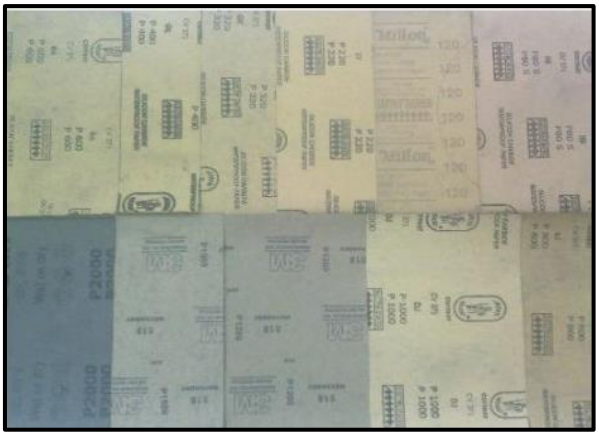

Figure 3.4: Abrasive papers.

3.4.4 Polishing

Polishing machine (Make: Struers, Danish) was used to obtain a scratch free and mirror finish surface. Polishing was carried out using soft cloth (velvet, canvas, suede or selvet etc.) and a polishing medium (diamond paste). Before the start of polishing, the polishing cloth was thoroughly washed with water to remove any contaminants which may cause surface damage. Further, the polishing medium was spread on to a well washed cloth and polishing was performed. The specimen was held on the rotating disc in order. Polishing machine was used in the present work. Figure 3.5 presents the schematic of polishing machine.

Figure 3.5: Polishing Machine (Courtesy: IIT, Bombay).

3.4.5 Electro-polishing

The electro polishing can be done on prepared samples so as to remove dust and scratches from the sample. Electro-polishing to be done with perchloric acid 20% and methanol 80% at

27V, 4.5A current for 10 sec. Figure 3.6 illustrates the electro-polishing machine utilized in the present work.

Figure 3.6: Electro-polishing (Courtesy: IIT, Bombay).

3.4.6 X-Ray diffraction (Bruker)

The X-ray Diffraction (XRD) is a rapid analytical, non-destructive system for analysing a large range of alloys, including metals, polymers and semiconductors. It has become an indispensable method for materials investigation, and characterization. Example areas of application include phase analysis, crystallography, structure and relaxation determination, texture and residual stress investigations. The Bruker X-ray is equipped with stepper motors with optical encoder to ensure extremely precise angular values [42]. Residual stress measurements for four samples i.e. as received, 20%, 40% and 60% reductions at their surfaces and through thicknesses at three points up to T/2 at equal distances is measured. Figure 3.7(a, b) presents the XRD measurement sample setup and Bruker machine respectively.

(a) (b)

Figure 3.7: (a) Sample set-up (b) Bruker machine [42].

3.4.7 Electron Back Scatter Diffraction (EBSD)

Electron Backscattered Diffraction (EBSD) is a technique which allows crystallographic information to be obtained from samples in the scanning electron microscope (SEM). In EBSD, a stationary electron beam strikes a tilted crystalline sample and the diffracted electrons form a pattern on a fluorescent screen. This pattern is characteristic of the crystal structure and orientation of the sample region from which it was generated. The diffraction pattern is used to measure the crystal orientation, grain boundary misorientations, identify different materials, and provide information about local crystalline perfection. When the beam is scanned in a grid across a polycrystalline sample and the crystal orientation measured at each point, the resulting map reveals the constituent grain morphology, orientations, and boundaries [43]. In the present study, EBSD was used to get the orientation of grains in which cold rolling was done. All the EBSD measurements were taken on Quanta 3D FEG machine using OIM EBSD package keeping the parameters identical between scans as shown in Fig. 3.8.

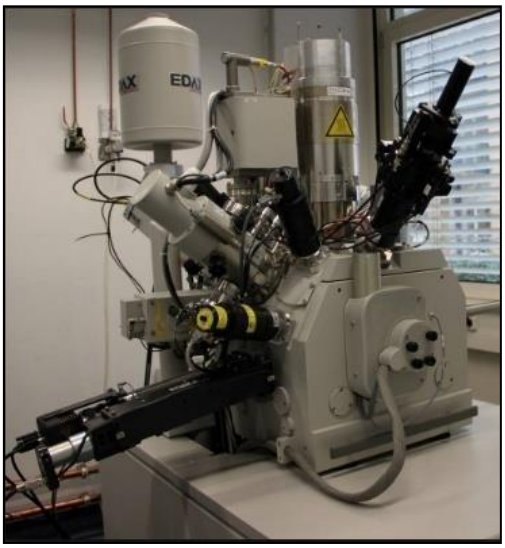

Figure 3.8: EBSD setup (Courtesy: IIT, Bombay).

3.5 Summary of this chapter

This chapter describes the objective, methodology, and equipment used for the experimental work. In the last section, details of different instruments and facilities that played a major role in the characterisation of as received material.

Chapter 4

Finite Element Modelling

4.1 Physical Description of the FE Model

A three dimensional, elasto-plastic finite element model was developed for cold rolling. The simulations were conducted in Abaqus™, a commercial simulation package. In the experiments, an elasto-plastic deformable rectangular titanium sheet with 150 mm in length, 100 mm in width and 8.4mm in thickness passes through two rolls. The rolls were 180 mm in diameter and rotating at a uniform rotational speed of 10 rpm. The rolls were modelled as discrete rigid and the sheet was taken as an elasto-plastic body. The experiments as well as simulations were conducted for 20%, 40% and 60% deformation (see Figure 4.1). The rectangular sheets with initial thickness of 8.4 mm were reduced to 6.72 mm, 5.04 mm and 3.36 mm respectively during the cold rolling. An elasto-plastic model was used in the present study to calculate the through thickness residual stress distribution during cold rolling. Abaqus™ allows using both implicit and explicit method for the simulations. Implicit method requires more time than explicit. Also, implicit method deals with static problems but it is not appropriate for large deformation problems such as rolling. Hence, explicit method was used for the simulation as it takes less time to calculate the results. A complete-two roll assembly has been used in the simulation. Simulations were performed with one pass, two pass and three pass for 20%, 40% and 60% reduction respectively. Coulomb friction was provided at the contact surfaces of roller and sheet. It is important to note that an adequate friction is required to ensure the roll bite occurs. The frictional forces at the interface of the roll and the sheet are responsible for pulling the sheet through the rolling mill. In the entry zone, the roll moves faster than the sheet whereas in the exit zone, the rolled sheet moves faster than the roll. As a result, a residual stress gradient developed across the thickness of the rolled sheet. In addition, the effect of rotational speed on through thickness gradient has also been investigated in this thesis.

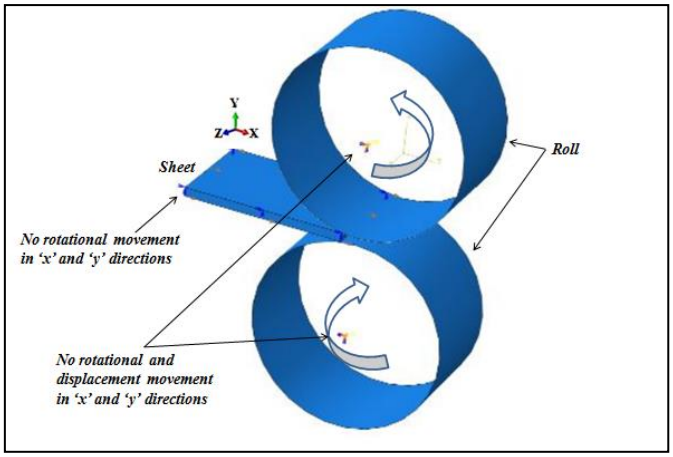

Figure 4.1: A three dimensional, elasto-plastic finite element model for 20%, 40% and 60% deformation.

4.2 Numerical Formulation

The geometric model used a three-dimensional continuum stress/displacement, 8-noded linear brick, and C3D8R elements. A structural meshing technique for the discretization of the model is used. Abaqus/Explicit provides three different options for C3D8R elements i.e. average strain kinematic, orthogonal and centroid formulations. The average strain kinematic formulation and the default hourglass control were used in this work. Though, average strain kinematic formulation required more computational time compared to other two formulation technique. It was preferred due to more accuracy of the results. Built-in hourglass control method was used in this study to avoid spurious deformation of the mesh. An optimum meshing is required for proper computational time. The model used in this study has 37800 elements and 39980 nodes with 42, 30 elements in thickness width direction respectively. A non-uniform, double biasing (with bias ratio 3) mesh was generated in the thickness direction as shown in Figure 4.2.

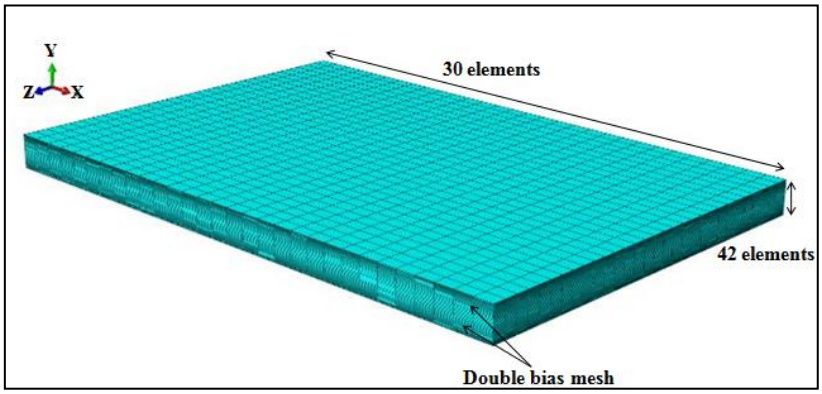

Figure 4.2: Meshing of sheet.

4.3 Material model

For the isotropic model, Young's modulus of elasticity (E) and Poisson's ratio (ν) were taken to be 115 GPa and 0.31, respectively [41]. The plastic data was used in a tabular form to define the flow stress model as seen in Table 4.3, which follows the stress-strain curve behaviour as shown in Figure 4.3.

Table 4.1: Plastic flow stress [42].

Yield Stress (MPa)	Plastic Strain
1020	0
1040	0.004
1050	0.03
1070	0.062
1030	0.066

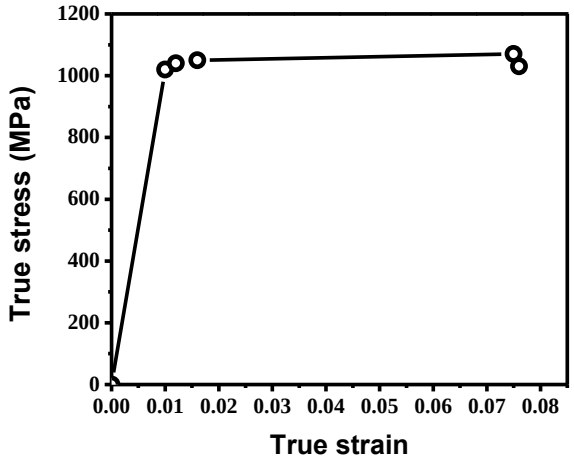

Figure 4.3: Stress-strain curve for commercial pure titanium [42].

4.4 Boundary and Contact Conditions

Boundary conditions were divided into two steps; an initial step and the analysis step**.** In the initial step, the sheet was given an initial velocity of 0.8 mm/s in x-direction. The interaction between the roller and the outer surface of the sheet was defined in this step. A displacement/rotation boundary condition was defined to constrain the motion of the sheet. The side faces of the sheet were made zero in 'x' and 'z' direction. Similarly, the boundary condition for both the rollers was made such that the rollers could rotate only about their

respective axis of rotation. All other translational and rotational degrees of freedom were constrained in ‘x’ and ‘z’ directions as shown in Figure 4.1. In the analysis step, the rollers were given with an equal and opposite angular velocity. The friction model used in this study, allows the relative motion between the two contact surfaces. The frictional coefficients values used in the simulations were varied from 0.25-0.6.

4.5 Residual stress evolution

To achieve the residual stress state in a deformed rolled sheet, it is necessary to give a sufficient relaxation time for elastic recovery. This was achieved by providing 7-time steps as relaxation period for 20% deformation, 13-time steps as relaxation period for 40% deformation and 20-time steps as relaxation period for 60% deformation as shown in Figure 4.4.

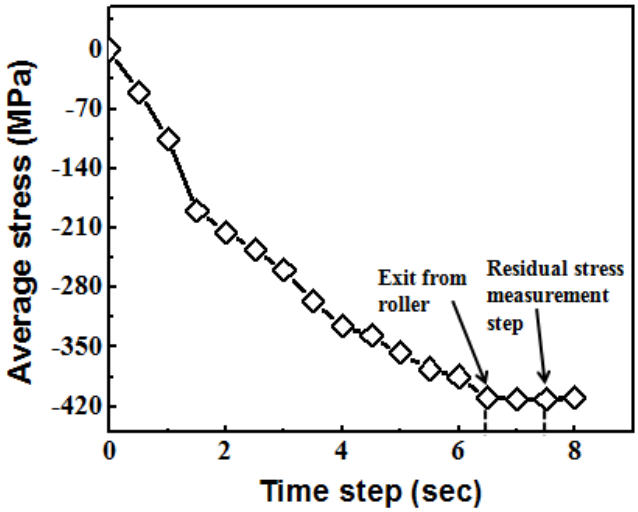

Figure 4.4: Residual stress measurement step.

4.6 Mesh sensitivity

Element size plays an important role in attaining accurate results. The large number of elements can increase the computational time and a very small number of elements can lead to the inaccurate results. Therefore, determining optimal element size is must for carrying out the simulation effectively. Simulations were done using different mesh sizes and the number of elements in the model ranged between 33000 and 40000. It can be seen in Figure 4.5 that the maximum stress values saturate at 37800 elements. The optimal mesh size corresponding to 37,800 elements (shown by vertical line) was used in the rolling simulations.

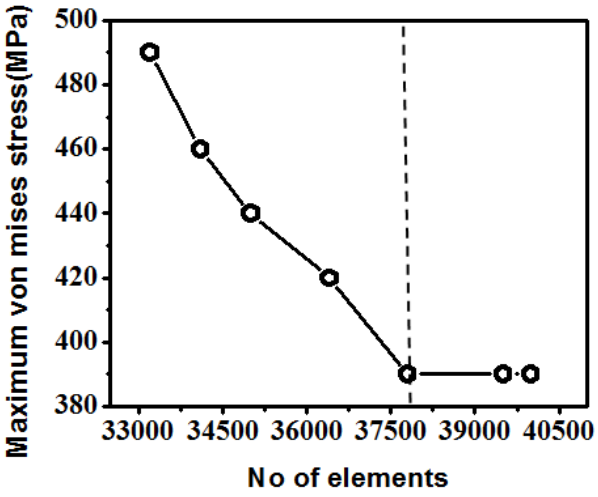

Figure 4.5: Mesh sensitivity analysis.

Chapter 5

Results and Discussion

5.1 General

The chapter presents the characterisation and testing results obtained for grade-2 titanium alloy. The chapter describes the various EBSD and residual stress analysis obtained for different thickness reductions 5%, 20%, 40%, and 60% at different thickness locations T0, T/7, T/4, T/2 respectively.

5.2 Through-Thickness Microstructural Development

The through-thickness microstructural developments are described in terms of gradients in grain structure and residual stress. These are shown one by one in below.

5.2.1 Gradients in Grain Structure:

The EBSD data were analysed to get indication of the rolling induced deformation gradients: in grain size (Fig. 5.1a). Grain size reduced with increasing rolling reductions. Increased rolling reductions also lead to elongation of grains and increased the fraction of the non-indexed points.

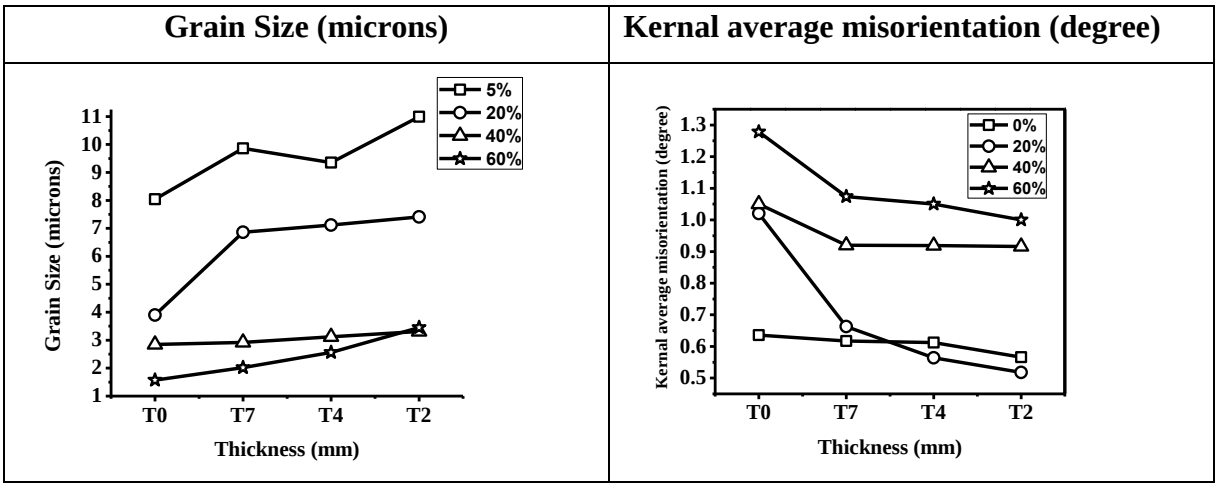

(a) (b)

Figure 5.1: EBSD data for different thickness locations T0, T/7, T/4, T/2 (a) Grain size and (b) kernel average misorientation (KAM).

All these were, however, non-uniform across the thickness of the rolled sheet: a clear indication of the through thickness deformation gradients. The indication of the through thickness deformation gradients were also observed on the local misorientation developments (see Fig. 5.1b) for the kernel average misorientation (KAM).

5.2.2 Gradients in residual stress:

The multiple {hkil} XRD method was used to determine the residual stress development across the cold rolled sheet. As mentioned in section 3.5.6, this method considered all the available {hkil} poles for determining the both normal (σ_{11}) (Fig. 5.2a) and shear (τ_{13}) (Fig. 5.2b) components of the stress matrix. The stress distribution across the sheet thickness for different deformation percentage is plotted in Fig. 5.2.

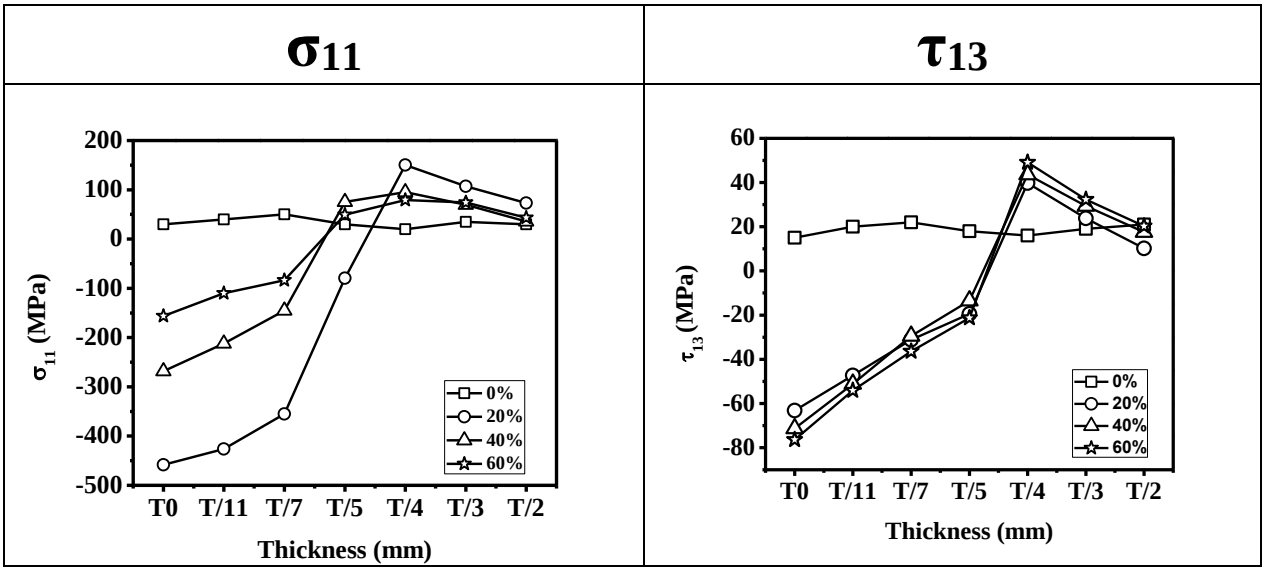

(a) (b)

Figure 5.2: Residual stress signatures as a function of thickness: (a) σ11 and (b) τ13.

As shown in Fig. 5.2, the starting material had negligible stress in it and did not show any deformation gradient. However, a clear demarcation in the stress values of both σ_{11} and τ_{13} established a gradient. A highly compressive residual stress has been observed on the surface (T0) of the specimen which changes to tensile at T/4 and a reduction in stress was observed afterwards (see Fig. 5.2). The increase in the deformation percentage leads to near surface (T0) stress relaxation from -435 MPa to -156 MPa (see Fig. 5.2a). However, τ_{13} component showed a marginal increase from -63 MPa to -75 MPa (Fig. 5.2b). The stresses became

tensile at T/4. The σ_{11} component showed a highest tensile stress for 20% reduction (Fig. 5.2a). On the other hand, τ_{13} showed a marginal increase from 39MPa to 49MPa (Fig.5.2b). The difference in stress values with deformation seems to be marginal for both σ_{11} and τ_{13}. The material was characterized till mid-thickness (T/2) of the sheet due the symmetric nature of the rolling. The σ_{11} stress varied from 35 MPa to 63 MPa and τ_{13} from 10MPa to 20 MPa on mid-thickness (T/2) of the rolled sheet.

5.3 Process characterization via Finite Element Simulations

5.3.1 Evolution of through thickness plastic strains:

The finite element analysis was used to observe the deformation gradient developed during rolling. These were then compared with the experimental results. The parameters kept constant between the experiments and the simulations. Though, the full sheet was rolled, only half-section of the sheet was used for the analysis. The upper surface (T0) of the sheet showed higher plastic strain (von mises and shear strain) in comparison to the mid-thickness (T/2). The plastic strain decreased from T0 towards T/2 and become saturated between T/5 & T/3 (Fig. 5.3a). The highest strains on the top surface may be due to the direct contact between the sheet and the roll assembly. This result in bulk plastic metal flow of the material. A similar variation in material plastic flow was observed through plastic strain signature of the experimental microstructure (Fig. 5.3a). The percentage change in von mises effective strain and shear strain is 12% and~98% respectively. The shear strain distribution showed a significant reduction from T0 to T/2. A clear deformation gradient has been established through simulations and was validated with the observed microstructural gradient (Fig 5.3b). This gradient can be explained through the experimental measurable residual stress development through the rolled sheet.

Strain / %Deformation	Effective von mises strain	Shear strain ε_{12}
20%	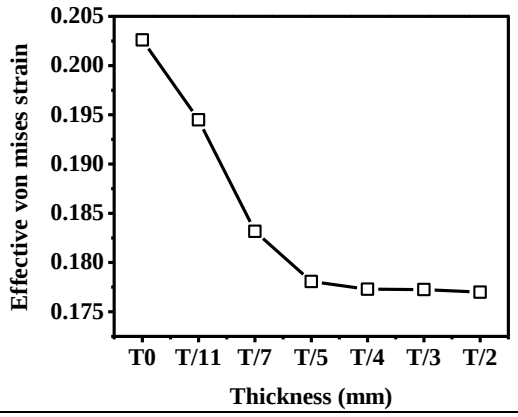	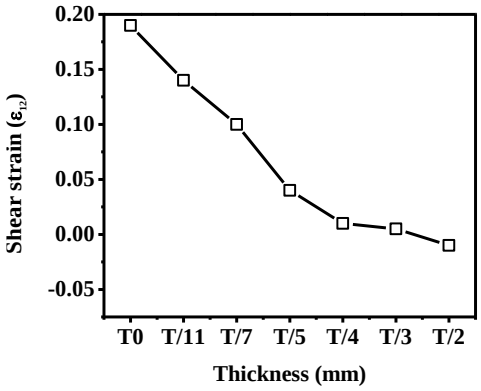
40%	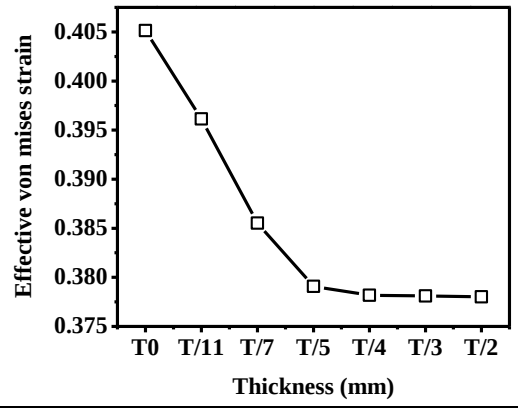	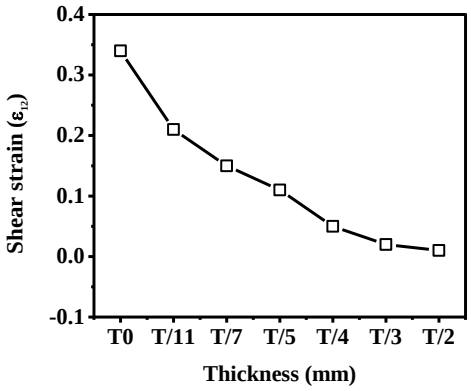
60%	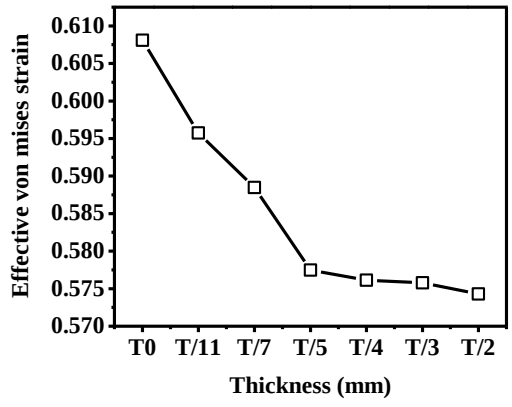	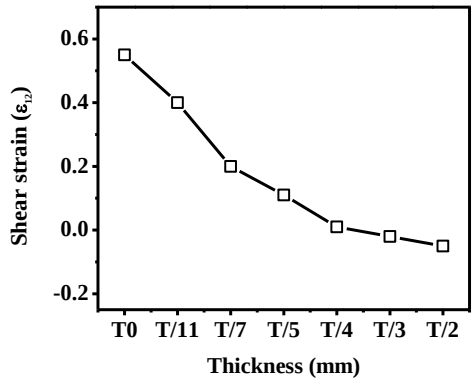

(a) (b)

Figure 5.3: Validation of the experimental results from simulation: through thickness (a) plastic strain and (b) shear strain gradients.

5.3.2 Evolution of through thickness residual stresses:

Figure 5.4 shows the comparison of experimental and simulated residual stress results. The stress gradient is more on the surface and sub surface of the sheet and insignificant on the mid-thickness. However, a force balance between the surface and the mid-section is maintained. The experimental measurements showed a tensile nature of the stresses at the mid-thickness of the rolled sheet, the simulations provided a compressive stress. This could be due to isotropic assumption taken while conducting the FEM simulations. An error percentage of 25 was considered to be acceptable to validate the experimental and simulations results. This showed the effectiveness of the model to capture the stress gradient in σ_{11} component of the stress matrix.

Stresscomponents / %Deformation	σ_{11}(MPa)	τ_{13} (MPa)
20%	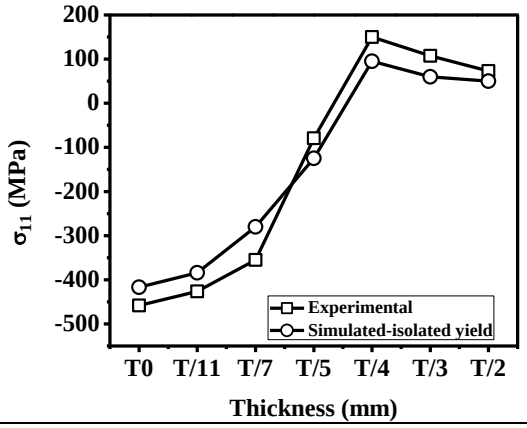	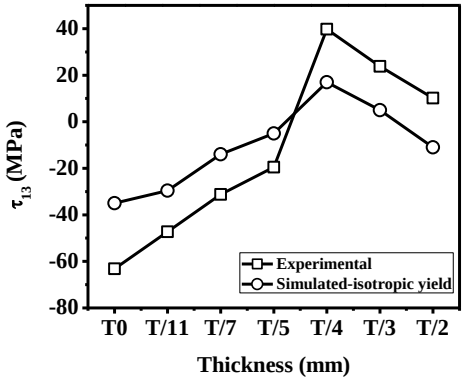
40%	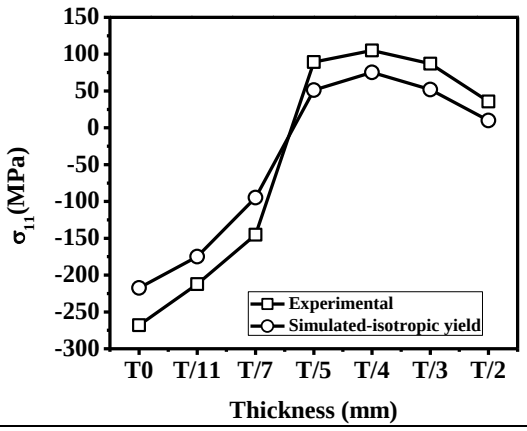	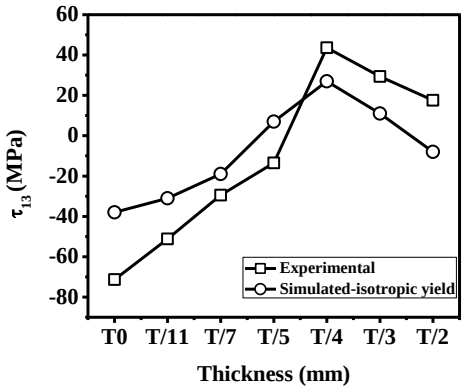
60%	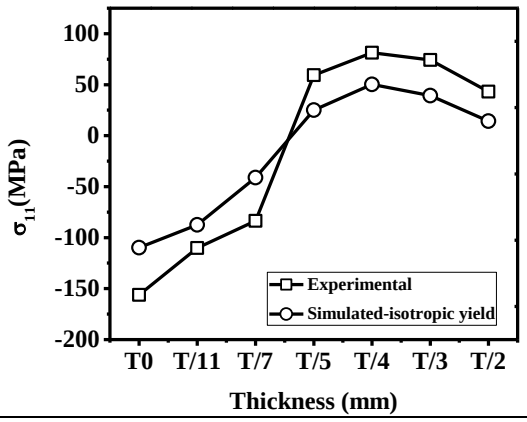	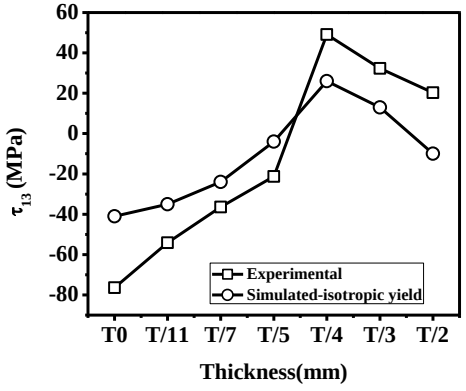

Figure 5.4: Comparisons between experimental and simulated of through thickness residual stress gradients. The comparisons were made both for σ_{11} and τ_{13} components.

5.3.3 Effect of process variables on residual stresses:

Since the numerical model was observed and verified with residual stresses, it was determined to vary different process variables like: coefficients of friction (COF) (see Fig. 5.5) and rotational speed (see Fig. 5.6) in order to expand the simulations. The simulation results are calculated for σ11 and it was observed that the patterns of through thickness residual stress gradients did not vary both with change of COF or the rotational speed. However, there were considerable differences in the values of thicknesses when these graphs were compared for example; the residual stresses at the surface (T0) appeared to become more compressive at the low rolling reductions. This was due to the relaxation of stresses and dynamic recovery at higher reductions. Rolling speed and COF enhanced the residual stress gradients, the magnitude of compressive residual stresses and sub-surface peak tensile stresses increased with rolling speed and COF irrespective of the deformation percentage.

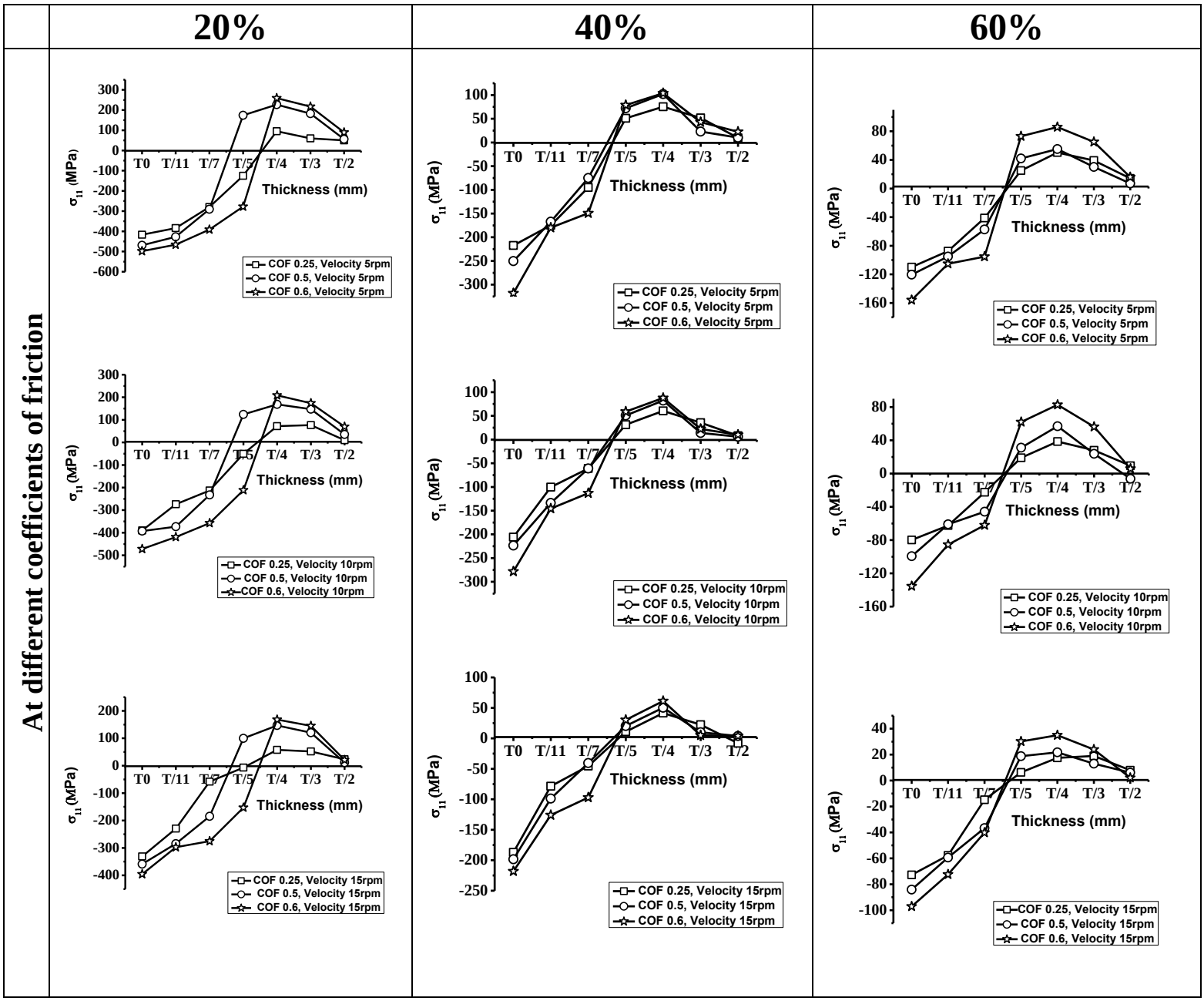

Figure 5.5: Effect of process parameter COF on the residual stress gradient. The values of COF speed varied from 0.25-0.6 at a constant roll diameter of 180mm with sheet initial velocity equal to 0.8 mm/s.

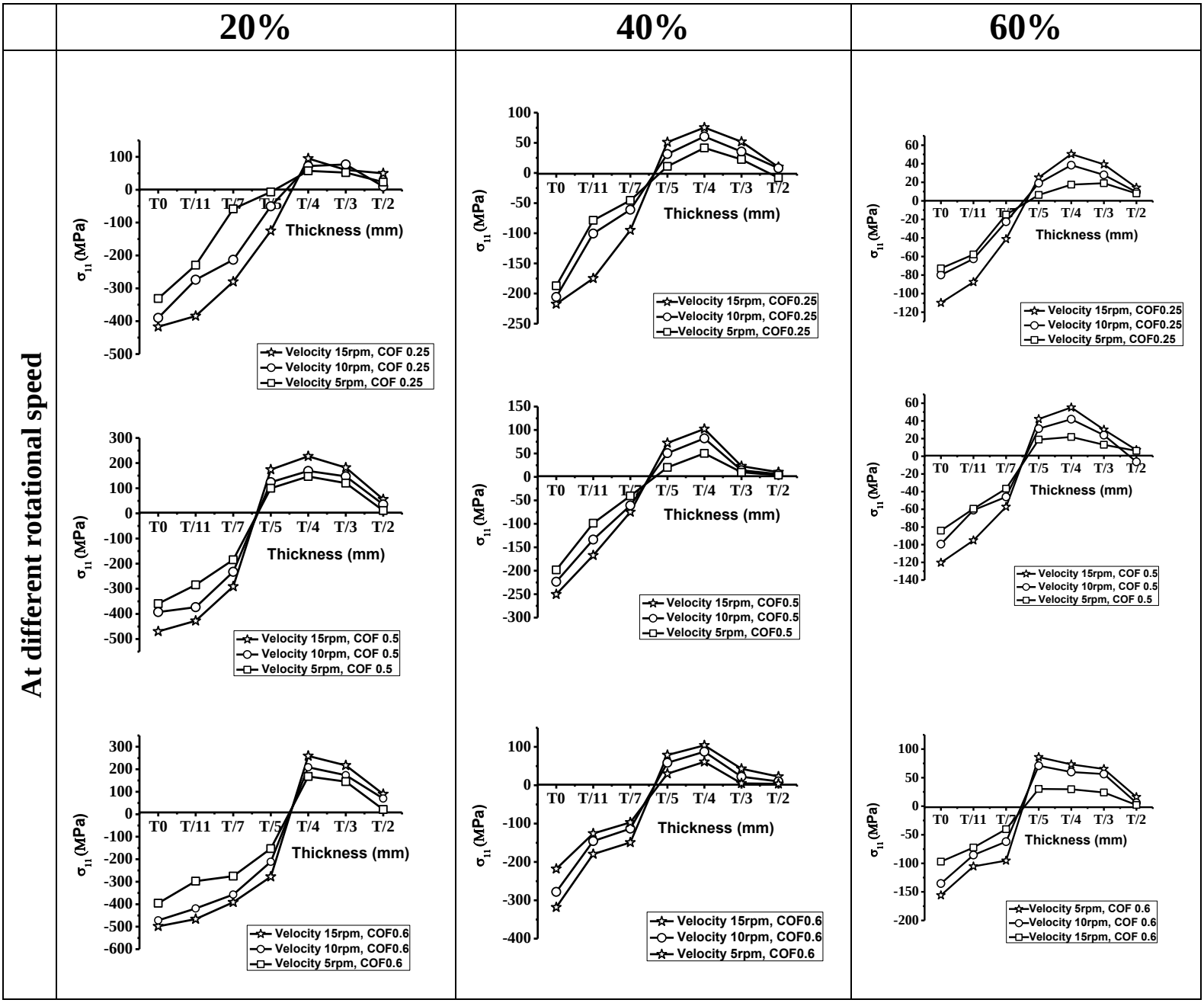

Figure 5.6: Effect of process parameter rotational speed on the residual stress gradient. The values of rotational speed varied from 5-15rpm at a constant roll diameter of 180mm with sheet initial velocity equal to 0.8 mm/s.

Chapter 6

Conclusion and Scope of Future Work

6.1 Conclusions

This chapter concludes the results obtained from various experiments performed during the present research. Initially, the results obtained from microstructure and residual stress analysis was discussed. Titanium sheet (of 8.4 mm thickness) was subjected to 20%, 40% and 60% thickness reductions by cold rolling. Experimental measurements were made to establish through thickness evolution in microstructure and residual stress. Numerical simulations were made to establish through thickness gradients in strain and in residual stresses. Following are the main observations:

1. An elastic-plastic finite element simulation provided clear through-thickness gradients in (von Mises and shear) strain. The plastic strain decreased from T0 towards T/2. The upper surface (T0) of the sheet showed higher plastic strain in comparison to the mid-thickness (T/2).
2. Comparison between the simulated and experimental measurements was possible for the residual stress. Both experiments and simulations showed similar trends: near surface compressive residual stresses turning tensile at T/4, while between T/4 and T/2 relief in stress.

6.2 Scope of future work

1. The effect of twinning on residual stress distribution.
2. Correlation between texture development and residual stress distribution.
3. Numerical study of stress gradient during cold rolling of titanium alloy using anisotropic yielding.
4. Effect of roll geometry on the through thickness residual stress gradient.

References

1. Verlinden, B., Driver, J., Samajdar, I., and Doherty, R.D, (2007) Thermo-mechanical processing of metallic materials. *Pergamon materials series*.
2. Soul, F. and Hamdy, N. (2012) Numerical simulation of residual stress and strain behaviour after temperature modification. *Intech*.
3. Maawad, E.K.S., (2013) Residual stress analysis and fatigue behavior of mechanically surface treated titanium alloys. *HZG Report*.
4. Withers, P.J., (2007) Residual stress and its role in failure. *Report on Progress in Physics*, **70**, 2211–64.
5. http://www-ensped.utt.fr/aboutprestress/definition.htm (11/06/2017).
6. Withers, P.J., and Bhadeshia, H. K. D. H., (2001) Residual stress part 2 – Nature and origins. *Materials Science and Technology*, **17**, 366–74.
7. Sekar, C.K., and Sivagnanam M.N., (2007) Effect of heat treatement method in minimizing the residual stress level in cold drawn weldeed tubes. *Tube Net*.
8. Oh, H.J., and Song, S.K., (2017) Surface strengthening of injection moulded parts by applying a thermal insulation film. *Royal Society of Chemistry*.
9. Liou, J.J., and El-Wardany, T.I., (2014) Finite Element Analysis of Residual Stress in Ti-6Al-4V Alloy Plate Induced by Deep Rolling Process under Complex Roller Path. *International Journal of Manufacturing Engineering*, **2014.**
10. Yentzer, T., Stillman, B., Pardue, B., and Khaled, T., Fatigue life and residual stresses in cold rolled propeller blades.
11. Manouchehrifar, A., and Alasvand, K., Finite element simulations of deep rolling and evaluate the influence of parameters on residual stress.
12. https://en.wikipedia.org/wiki/Residual_stress (14/08/2016).
13. https://en.wikipedia.org/wiki/Titanium Sfgdb (28/09/2016)
14. https://www.rti titanium.com (21/08/2016).
15. Ahmed, Y.M., Sahari, K.S.M., Ishak, M., and Khidhir, B.A., (2014) Titanium and its Alloy. *International Journal of Science and Research*, **3**, 1351–61.
16. http://www.azom.com/article.aspx?ArticleID=915 (13/05/2017).
17. http://universalium.academic.ru/294934/Titanium_aerospace_alloys (17/12/2016).
18. https://en.wikipedia.org/wiki/Rolling_ (metalworking) Dsbs (20/10/2016).
19. https://en.wikipedia.org/wiki/Cold-formed_steel (20/11/2016).

20. http://www.ksprofile.com/benefits-roll-forming (15/11/2016).
21. Montmitonnet, P., (2006) Hot and cold strip rolling processes. *Computer Methods in Applied Mechanics and Engineering*, **195**, 6604–25.
22. http://dogamak.com/en/rolling-mills (23/06/2017).
23. Button, S.T., (2011) Numerical and experimental analysis of lubrication in strip cold rolling. *Journal of the Brazilian Society of Mechanical Sciences and Engineering*, **33.**
24. https://www.sail.co.in/applications (04/05/2017).
25. Yoo, (1981) Slip, twinning and fracture in hexagonal close packed metals. *Metallurgical Transactions A*, **12A**, 409–18.
26. Nourbakhsh, S., and O'brien, T., (1988) Texture formation and transition in cold-rolled titanium. *Materials Science and Engineering*, **100**, 109–14.
27. Blicharski, M., Nourkakhsh, S., and Nutting, J., (1979) Structure and properties of plastically deformed α-Ti. *Metal science*, **13**, 516.
28. Keeler, J.H., and Geisler, A.H., (1956) Preferred orientations in rolled and annealed titanium. *Transctions AIME*, **8**, 80–90.
29. Philippe, M.J., Esling, C., and Hocheid, B., (1988) Role of twinning in texture development and in plastic deformation of hexagonal materials, *Textures and Microstructures*, **7**,265–301.
30. Nishitani, S.R., Oh, M.H., Nakamura, A., Fujiwara, T., and Yamaguchi, M., (1990) Cold-rolling of Ti-rich TiAl polysynthetically twinned crystals. *Journal Material Research*, **5**, 484–87.
31. Chun, Y.B., Yu, S.H., Semiatin, S.L., and Hwang, S.K., (2005) Effect of deformation twinning on microstructure and texture evolution during cold rolling of CP-titanium. *Materials Science and Engineering*, **398**, 209–19.
32. Zhou, T.Q., Itoh, G., Motohashi, Y., and Niinomi M., (2006) Microstructural modification in a beta titanium alloy for implant applications. *Materials Transactions*, **47**, 90–5.
33. Bozzolo, N., Dewobroto, N., Wenk, H.R., Wagner, F., (2007) Microstructure and microtexture of highly cold-rolled commercially pure titanium. Journal Material Science, **42**, 2405–16.
34. Gonzalez, M., Pen, J., Manero, J.M., Arciniegas, M., and Gil, F.J., (2009) Optimization of the Ti-16.2Hf-24.8Nb-1Zr alloy by cold working. Journal of Materials Engineering Performance, **18**, 506-10.

35. Bao, L., Lecomte, J.S., Schuman, C., Philippe, M.J., Zhao, X., and Esling, C., (2011) Study of plastic deformation in hexagonal metals by interrupted in-situ EBSD measurement. *Soutenue le*.
36. Zherebtsov, S.V., Dyakonova, G.S., Salem, A.A., Malysheva, S.P., Salishcheva, G.A., and Semiatin, S.L., (2011) Evolution of grain and subgrain structure during cold rolling of commercial-purity titanium. *Materials Science and Engineering*, **528**, 3474-79.
37. Zhao, X., Niinomi, M., Nakai, M., and Hieda J., (2012) Effect of deformation-induced ω phase on the mechanical properties of metastable β-type Ti-V alloys. *Materials Transactions*, **53**, 1379–84.
38. Tripathi, M.K., Srinivas, N.C.S., and Singh, V., (2013) Effect of cold rolling on low cycle fatigue behaviour of a near alpha titanium alloy. International Journal of Research in Engineering and Technology, **02**, 345–48.
39. Wronski, M., Wierzbanowski, K., Baczmanski, A., Wronski, S., Bacorix, B., Wrobel, M., and Lodini A., (2014) Modification of stress and texture distributions in asymmetrical rolled titanium. *Advanced Materials Research*, **996,** 688–93.
40. Jaroslav, M., Frantisek, H., Jaroslav, V., Kamil, K., and Jiri, C., (2015) The effect of cold rolling of microstructure and mechanical properties of TI-35NB-6TA alloy. *Czech Republic*.
41. http://www.azom.com/properties.aspx?ArticleID=1547 (07/01/2017).
42. Anjum, Z., Qayyum, F., Khushnood, S., Ahmed, S., and Shah, M., (2015) Prediction of non-propagating freeting fatigue cracks in Ti6Al4V sheet tested under pin-in-dovetail configuration: experimentation and numerical simulation. *Materials and Design*, **87**, 750–58.
43. https://www.iitr.ac.in/centers/IIC/uploads/File/XRD.pdf (15/04/2017).
44. https://en.wikipedia.org/wiki/Electron_backscatter_diffraction (15/04/2017).